LIMITATIONS OF THE HYDROTALCITE FORMATION IN PORTLAND COMPOSITE CEMENT PASTES CONTAINING DOLOMITE AND METAKAOLIN

Alisa Machner[1,2,*], Maciej Zajac[3], Mohsen Ben Haha[3], Knut O. Kjellsen[1], Mette R. Geiker[2], Klaartje De Weerdt[2]

[1]Norcem AS, R&D Department, Setreveien 2, P.O. Box 38, 3991 Brevik, Norway
[2]NTNU Department of Structural Engineering, Richard Birkelandsvei 1A, 7491 Trondheim, Norway
[3]Heidelberg Technology Center GmbH, Oberklamweg 2-4, 69181 Leimen, Germany

*Corresponding author: alisa.machner@ntnu.no
+47 45394622
ORCID-ID: 0000-0002-6334-5116

ABSTRACT

This study focuses on the reaction of dolomite powder in combination with metakaolin in Portland composite cement pastes. We studied paste samples cured at 20 °C, 38 °C, and 60 °C for up to 1 year. In these systems, the only magnesium-containing hydration phase of dolomite observed was hydrotalcite. Dolomite reacted notably already after 90 days when cured at 60 °C, whereas at lower curing temperatures the reaction was limited. The increased availability of aluminium due to the addition of metakaolin did not contribute to the formation of hydrotalcite. The refined pore space due to the metakaolin addition did not inhibit the hydrotalcite formation. However, the almost total absence of portlandite due to the pozzolanic reaction of the metakaolin inhibited the dolomite reaction, even in pastes with high porosity. Portlandite seems to be the driving force for the reaction as its absence is inhibiting the reaction to take place.

Keywords: Thermal Analysis (B), X-Ray Diffraction (B), $Ca(OH)_2$ (D), Blended Cement (D), Dedolomitization Reaction

1 INTRODUCTION

Supplementary cementitious materials (SCMs) are frequently used as a partial substitute for cement clinker to reduce the emissions caused by cement manufacturing. However, some of the SCMs traditionally used have limited availability when compared to the global increase of cement demand [1]. Therefore, alternative SCMs need to be found that are available in sufficient quantity and show similar or even improved interaction with cement clinker hydration.

Limestone is commonly used as an SCM and, according to the European cement standard EN 197-1, it can replace up to 5%wt clinker in CEM I Portland cements and up to 35%wt in CEM II Portland-limestone cements [2]. Due to the additional carbonates, the stable AFm phases which form are hemi- and monocarbonate and not monosulphate. This change in phase stabilities results in the so-called "ettringite stabilization", because the sulphate-containing hydration phase ettringite does not transform to monosulphate when the sulphate sources (e.g. gypsum) are depleted. This stabilization of ettringite beyond sulphate depletion results in a relative increase in the volume of hydrates, a corresponding decrease in porosity, and an increase in compressive strength [3,4].

The limited aluminium content in Portland cements means this effect is somewhat limited [4], but it can be amplified if additional aluminium is provided to the system by adding aluminium-delivering SCMs [5–8]. In this study, we used metakaolin as a model material for industrially available calcined clays supplying silicates and alumina to the system. Metakaolin is also known to be a pozzolanic material. During its pozzolanic reaction, the silicates provided by the metakaolin react with the portlandite formed during the hydration of the Portland cement to produce additional C-S-H [9], and the aluminium provided by the metakaolin reacts with the portlandite to form additional AFm phases [5–8]. Moreover, the aluminium is also partly taken up by the C-S-H [10] and can lead to the formation of calcium aluminate silicate hydrate phases (C-A-S-H phases), as observed in composite cements containing slag, fly ash or metakaolin [11,12].

Because high-grade limestone required by EN 197-1 [2] is not sufficiently available in all parts of the world, various other carbonate sources are in the focus of ongoing research. One possible alternative carbonate source that has been studied is dolomite [13]. This is a double salt consisting of calcium, magnesium and carbonate ions with the formula $CaMg(CO_3)_2$ and can function as a source of CO_2 and magnesium. In the alkaline environment of cement paste, dolomite can undergo a so-called "dedolomitization reaction" [14–16]. In this reaction, dolomite reacts with portlandite to form brucite and calcite. However, Zajac et al. have recently shown that the reaction of dolomite in Portland cement paste results in the formation of a similar phase assemblage to that of limestone addition [17,18]. They further show that the magnesium originating from the dolomite reaction results in the formation of hydrotalcite [17,18] (in the present study given as $Mg_6Al_2(OH)_{18}{\cdot}3(H_2O)$, according to [19]), which can lead to an increase in the compressive strength [17,20].

The present study focuses on the reaction of dolomite powders in combination with metakaolin used as SCM in Portland cement-based pastes. Metakaolin is used as a model material for SCMs that provide Al and Si. The aim was to determine whether dolomite reacts in these Al-rich systems, and what the reaction products are. We also wanted to understand more about the rate-limiting factors of the dolomite reaction in these systems.

We investigated the phase assemblage and microstructure of hydrated cement pastes, in which 40%wt of Portland cement was replaced by various combinations of dolomite and metakaolin. The pastes were sealed-cured at 20 °C, 38 °C and 60 °C for up to 360 days. Elevated curing temperatures were applied to accelerate the reaction of the dolomite and to be able to study its reaction products. The following techniques were used to characterize phase assemblage and microstructure: XRD, TGA, SEM-EDS and MIP. The phase assemblage was compared with those of a plain Portland cement paste and systems containing limestone so that we could identify the effect of dolomite on the phase assemblage. In addition, a paste with a high w/b ratio, and well-hydrated samples exposed to additional portlandite and or water were prepared to study the impact of increased porosity or additional portlandite on the dolomite reaction.

2 EXPERIMENTAL

2.1 MATERIALS

The mixes investigated in this study were prepared using a Portland cement clinker (C) supplied by Norcem AS, natural dolomite (D) and limestone (L) supplied by Miljøkalk AS, and laboratory-grade metakaolin (M) supplied by Imerys (Metastar501) and gypsum supplied by Merck. The cement clinker was ground in a laboratory ball mill until a Blaine surface area of approx. 400 m^2/kg was achieved. The other materials were used as received. The chemical and mineralogical composition of all materials were investigated with XRF (Table 1) and QXRD (Table 2 and Table 3). It should be noted that the Portland cement clinker used shows a relatively high alkali content. The particle size distributions of the materials used were determined from the average of 3 independent measurements with laser diffraction (Malvern Mastersizer 2000E) (Figure 1).

The experimental matrix is given in Table 4. Taking into account the sulphate content of the clinker as determined by XRF, laboratory grade gypsum was added when preparing the mixes to achieve a sulphate content of 2.5%wt per gram of binder in all mixes. This sulphate level was determined by isothermal calorimetry at 20 °C on the sample with the highest metakaolin content. At a sulphate content of 2.5%wt, the secondary aluminate peak appeared after the silicate peak and thereby the system is assumed to contain sufficient amounts of sulphates. The sulphatation was, however, not checked at the elevated curing temperatures (38 °C and 60 °C). It should be noted that the values in Table 4 do not reflect the actual amounts in the mixes, as they do not include the amount of gypsum added to the system. A pure Portland cement (100C = ground Portland cement clinker + gypsum) was used as a reference. In the other mixes, 40%wt of the Portland cement clinker was replaced with metakaolin and or dolomite, or limestone. Paste samples were prepared in the laboratory at 20 °C with a w/b ratio of 0.45 for all mixes, and in the case of 60C20D20M, an additional paste sample was also prepared with a w/b ratio of 0.93. The

pastes were mixed in a BRAUN MR550CA high-shear mixer (speed 6) and cast in 12 ml plastic tubes (mixing procedure: mixing for 30 seconds, waiting for 5 minutes, mixing for 1 minute again). The sealed tubes were cured at 100% RH in a sealed box at 20 °C, 38 °C and 60 °C for up to 360 days and up to 400 days in the case of the samples prepared with the various w/b ratio samples. The curing at elevated temperatures (especially 60 °C) was used to accelerate the reaction of dolomite and to be able to study its reaction products.

Additionally, two tubes of the samples with the highest metakaolin content (20%wt) and the w/b ratio of 0.45 were exposed to additional portlandite and or water after a curing time of 1 year and 9 months (approx. 630 d) at 60 °C. We crushed the samples to a particle size between 1 mm and 0.25 mm and filled them in 45 ml centrifuge tubes. To both samples 30%wt of deionized water and to one of them additional 30%wt of portlandite were added. These samples were stored again sealed at 60 °C at 100% RH and investigated after 28 and 90days.

2.2 METHODS

Prior to the investigation of the phase assemblage of the cement pastes using thermogravimetric analysis (TGA) and X-ray diffraction (XRD), the hydration was stopped by double solvent exchange after 28, 90, 208 and 360 days of curing. The samples prepared with the different w/b ratio were stopped after 400 days of curing. For this, a 6 mm thick slice (diameter: 23 mm) was cut off each cured cement paste sample. This slice was crushed in a porcelain mortar until the whole sample had passed through a 1 mm sieve. The coarsely crushed cement paste was then immersed in 50 ml isopropanol, shaken for 30 seconds, and left to rest for 5 min before the isopropanol was decanted. This isopropanol treatment was performed twice before the sample was transferred to a filtration unit where the isopropanol was filtrated out and the paste was immersed in 10 ml petroleum ether. After 30 seconds of stirring, the suspension was left to rest for 5 minutes. The sample was then vacuum-filtrated and subsequently dried. The 28-day-old samples were dried for 15 min in an aerated oven at 40 °C. All other samples were dried overnight

in a desiccator under a slight vacuum (-0.2 bar) applied using a water pump. After drying, the samples were crushed in a porcelain mortar until the whole sample passed through a 63 µm sieve. All samples were stored in a desiccator over silica gel and soda lime until measurement. The well-hydrated samples exposed to additional water and or portlandite were treated similarly with the difference that they have already been crushed at exposure and, due to the additional water, the amounts of isopropanol and petroleum ether were increased to 100 ml and 20 ml respectively. These samples were stopped after 28 and 90 days of exposure and directly prior exposure.

For the TGA measurements, the resulting dry powders were poured into 600 µl corundum crucibles and stored in a sample changer until measurement. The weight loss was measured from 40 °C to 900 °C with a heating rate of 10 °C/min in Mettler Toledo TGA/SDTA851 and TGA/DSC3+ devices. During the measurement, the measurement cell was purged with 50 ml/min of nitrogen gas. Both devices used a similar measurement principle and were operated with the same parameters. We, therefore, assume no significant differences between the results obtained from the two devices.

The derivate curves of the TG signal, the DTG curves, were used to detect phase changes. The DTG curves can be divided into several sections, in which the decomposition of specific phases can be detected as a weight loss. The first peak at around 100 °C is related to the ettringite decomposition and the beginning of the dehydroxylation of the C-S-H phase. C-S-H decomposes gradually between 40 °C and 600 °C [21] and appears as a polynomial baseline under the other peaks. The region between approx. 150 °C and 400 °C represents the stepwise dehydroxylation of the AFm phases (monosulphate, hemi- and monocarbonate) and other lamellar phases, including hydrotalcite (Ht). Consequently, there are several mass loss peaks visible in this temperature range. Hydrotalcite shows two mass loss events, the first at approx. 270 °C and the second at around 400 °C [21]. The subsequent sharp peak between approx. 400 °C and 550 °C is related to the decomposition of portlandite (CH). Above 550 °C carbonates decompose by emitting CO_2.

TGA was used to quantify the mass losses of various hydration phases, such as portlandite and hydrotalcite. The mass loss of a phase in a specific temperature interval can be determined by

integration of the derivative curve with subtraction of the background by a linear baseline as described by Lothenbach et al. [21]. The calculated weight losses were then normalized to the sample weight at approx. 550 °C, which was assumed to be the dry binder weight, and remained constant during the cement hydration, or to the original percentage of clinker in the sample (100%wt or 60%wt).

For the XRD analyses, the powder was loaded into the sample holders by means of front-loading and stored in a sample changer until measurement. For the measurements, we used a D8 Focus diffractometer from Bruker with a Bragg-Brentano θ–2θ geometry and a goniometer radius of 200.5 mm. The samples were measured between 5 °2θ and 55 °2θ with a step size of 0.01 °2θ and a sampling time of 0.5 seconds per step. We used Cu-Kα radiation with a wavelength of approx. 1.54 Å as the X-ray source. The XRD plots were qualitatively evaluated with the DIFFRAC.EVA V4.0 software from Bruker by using the PDF4+ database from ICDD and the COD database. For the quantification of the dolomite content in the samples (QXRD), the TOPAS 5 software from Bruker was used combined with the G-Factor Method [22, 23] was applied by using an external quartzite standard. The quartzite was calibrated against a silicon powder from NIST (Standard Reference Material 6640d). For the C-S-H phase, the model described by Bergold et al. was used in the refinement [24].

To investigate the phase assemblage and microstructure of the samples with scanning electron microscopy (SEM), a 3 mm slice was cut off the cured cement paste and immersed in isopropanol for min. 1 week. Then the slice was dried, cast in epoxy and polished. In case of the well-hydrated samples exposed to additional water and portlandite, parts of the samples from the double solvent exchange as described above before grinding were used for polishing. We analysed polished and carbon-coated sections of selected paste samples with the SEM. Elemental mapping and point analyses were carried out using a Hitachi S-3400N microscope equipped with an energy dispersive spectrometer (EDS) from Oxford Instruments.

To study the threshold pore entry diameter and total porosity of the paste samples with mercury intrusion porosimetry (MIP), a 7 mm slice was cut off the cured cement paste and coarsely

crushed in a porcelain mortar. The crushed samples were then immersed in isopropanol for at least 24 h and then dried in an aerated oven overnight at 40 °C to remove the isopropanol. For the MIP measurements, we used a Pascal 140/440 porosimeter from ThermoFisher Scientific and defined a contact angle of 140 °. The first intrusion curve reported from the measurements was used to determine the threshold pore entry diameter and the porosity of the samples. The threshold pore entry diameter was defined as the intersection of two tangents on the intrusion curve as described in [25]. The porosity as percentage of the sample volume equals the total porosity measurable with MIP and is determined by the maximum of the intrusion curve.

3 RESULTS

3.1 Quantification of the dolomite reaction

3.1.1 QXRD

QXRD was used to quantify the amount of unreacted dolomite in the hydrated cement paste samples. However, the hardness of the dolomite used in this study resulted in coarse dolomite particles in the powder even after grinding and therefore in the vertical exaggeration of one reflex of dolomite in the XRD-patterns (commonly called spottiness-effect). This effect resulted in a relatively large error in the quantification (estimated at approx. 10%wt). The results are given as the amount of dolomite determined by QXRD compared to the original amount of dolomite added. The theoretical amount of dolomite added equals the amounts given in Table 4. However, this is not the actual amount of dolomite added, because we also added gypsum to all the samples and the dolomite used contains approx. 90%wt of dolomite (Table 2).

After 360 days, the amount of dolomite was determined for all the mixes investigated. Figure 2 shows that the samples cured at 20 °C and 38 °C still contained a high amount of dolomite, close

to the actual amount of dolomite added, independently of the sample composition. However, when cured at 60 °C, the samples with low metakaolin contents, especially the sample 60C40D, showed a notable decrease in the amount of dolomite. For samples with a higher metakaolin content, the determined amounts of dolomite were again close to the actual amount of dolomite added.

Figure 3 shows the amount of dolomite in sample 60C40D over a period of one year. Samples cured at 20 °C and 38 °C showed a similar amount of dolomite, which was close to the actual amount of dolomite added. There is only a slightly increasing trend in the degree of reaction with curing time. For the samples cured at 60 °C, however, the amount of dolomite decreases significantly between 90 and 208 days and stayed rather constant afterwards.

Based on the QXRD results, the degree of dolomite reaction, therefore, seems to depend on the curing temperature, the curing time and the metakaolin addition.

3.1.2 SEM-EDS

Figure 4 and Figure 5 show the BSE images for the 60C40D and 60C35D5M samples, which showed the lowest amount of dolomite and therefore the highest degree of dolomite reaction with QXRD, cured at 60 °C for 1 year. Figure 6 shows the BSE image for the 60C20C20M sample, which showed limited dolomite reaction, cured under the same conditions. Alongside the BSE images, the figures show the corresponding elemental maps of magnesium, aluminium, oxygen, calcium and silicon for each sample.

The BSE images show large, uniformly grey particles, which the elemental maps show are rich in Mg and Ca, but poor in Al and Si. These particles are unreacted dolomite grains (up to approx. 70 µm in length). In the samples where dolomite has reacted, a clear reaction rim filled with Mg-rich reaction products can be observed around these grains (Figure 4 and Figure 5). The shape of the original dolomite grains is still visible in the BSE images, because it is marked with a thin layer of C-S-H precipitated around them, presumably at early ages, which then persisted even after the dolomite started to react at later ages. In addition to the larger, partially reacted dolomite grains

in these samples, small fully-reacted dolomite grains can also be observed (some indicated with arrows). They are completely filled with the Mg-rich reaction product and are surrounded by the C-S-H rim, which indicates the original dolomite grain boundary.

Figure 7 gives the BSE images for the samples 60C20D20M, which showed limited dolomite reaction under QXRD examination. Here we prepared two samples with the same binder, one with a w/b ratio of 0.45 and the other with a higher w/b ratio, namely 0.93. We did this to investigate the impact of increased porosity on the reaction of dolomite. As expected, the sample with the high w/b ratio shows considerably more porous microstructure than the sample with the lower w/b ratio (0.45). Moreover, significantly fewer unreacted clinker grains are visible in the high w/b sample than in the low w/b sample. However, the dolomite grains do not show any significant reaction in either case. So we conclude that the higher w/b ratio enhanced the clinker reaction, but was not able to enhance the dolomite reaction.

3.2 Phase assemblage

3.2.1 SEM-EDS

The elemental maps for the 60C40D and 60C35D5M samples cured at 60 °C for 1 year (see Figure 4 and Figure 5) show that the reaction rims inside the former dolomite grains are rich in magnesium, aluminium and oxygen, but that they do not contain calcium or silicon. This indicates that the product of the dolomite reaction contains magnesium and aluminium and its increased oxygen level indicates that it is a hydrate. Outside the former grain boundaries of the dolomite, no significant amount of magnesium could be detected by elemental mapping. This indicates that the magnesium-containing product of the dolomite reaction formed only within the former grain boundaries, indicating a low mobility of magnesium in the cement matrix, as reported in the literature [1]. Point analyses were performed to further identify the reaction product of the rim inside the former dolomite grains. When the results are plotted as the Mg/Si ration over the Al/Si

ratio, the data points describe a linear line for both samples (Figure 8). This indicates that the reaction product has a fixed Mg/Al ratio (the slope of the line). The small amount of Si present in the analysis originates probably from intermixing with other phases in the analysed volume. The reaction product can, therefore, be identified as hydrotalcite ($Mg_6Al_2(OH)_{18}{\cdot}3(H_2O)$) [26]. The Mg/Al ratio of the hydrotalcite was approx. 3.2 in sample 60C40D and 2.4 in sample 60C35D5M. In cementitious systems, Mg/Al ratios of approx. 2 are reported [17,26–30]. However, higher Mg/Al ratios are possible as well, as the natural mineral hydrotalcite has a Mg/Al ratio of 3 [31].

SEM-EDS point analyses also allow us to investigate changes in the C-S-H, e.g. aluminium uptake and changes in the Si/Ca ratio. The dot plots for C-S-H phase of the samples 60C40D, 60C35D5M and 60C20D20M cured at 60 °C are given in Figure 9. The Al/Si ratio can be determined from the slope of the lower lines, which are framing the C-S-H data clouds. While the addition of 5%wt metakaolin does not seem to change the C-S-H composition significantly (60C35D5M, Al/Si: 0.04) compared to the 60C40D sample (60C40D, Al/Si = 0), the addition of 20%wt metakaolin shifted the C-S-H composition to a considerably higher aluminium content (60C20D20M, Al/Si: 0.32). Simultaneously, the Si/Ca ratio is increased as well in this sample.

3.2.2 XRD

The XRD-patterns in the range of 8 to 12 °2θ for samples cured for 90, 208 and 360 days at 20 °C are given in Figure 10, for samples cured at 38 °C in Figure 11, and for samples cured at 60 °C in Figure 12. The figures indicate the main reflections of ettringite (Et, 9.1 °2θ), monosulphate-12H (Ms_{12}, 9.9 °2θ), hemicarbonate (Hc, 10.8 °2θ), hydrotalcite (Ht, 11.4 °2θ) and monocarbonate (Mc, 11.7 °2θ). Strätlingite (7.1 °2θ) was not detected in any of the samples, irrespective of curing temperature.

For the samples cured at 20 °C, dolomite seems to stabilize the ettringite (Figure 10), because all the dolomite-containing samples show a clear ettringite peak, but the 100C sample, which

302 contains no dolomite, does not. This is in line with the findings from Zajac et al. [17]. For the 100C
303 sample, the phases observed are monosulphate and some hemicarbonate, the latter possibly
304 formed by carbonation during queuing in the diffractometer. In the 60C40D sample,
305 monocarbonate is the main AFm phase. The sample containing 5%wt metakaolin (60C35D5M)
306 has a phase composition similar to the 60C40D sample. When the metakaolin content is increased,
307 e.g. from 5 to 20% (60C35D5M to 60C20D20M), small peaks of hemicarbonate are detected as
308 well. This can be explained by the increased aluminium provided by the metakaolin, which lowers
309 the CO_2/Al_2O_3 ratio and leads to the formation of hemicarbonate [32]. However, the
310 hemicarbonate peaks decrease over time due to the slow reaction of the dolomite, which slowly
311 increases the CO_2/Al_2O_3 ratio in the sample which stabilizes monocarbonate over hemicarbonate.
312 Additionally, there is a decrease in the intensity of the AFm peaks in the XRD-pattern. This could
313 be due to increased uptake of Al by C-S-H with increased metakaolin content, as shown by SEM-
314 EDS in Figure 9, which would leave less aluminium to form AFm phases. Hydrotalcite showed a
315 shoulder on the low-angle side of the monocarbonate peaks at 20 °C but no clear peaks.
316 The samples cured at 38 °C (Figure 11) show similar phase assemblages to those of the samples
317 cured at 20 °C. In the 60C40D sample, the monocarbonate observed is partially replaced by
318 hydrotalcite over time. The sample containing 5%wt metakaolin (60C35D5M) has a similar phase
319 composition to that of the 60C40D sample, but the hydrotalcite appears not as a clear peak, but
320 rather as a shoulder on the monocarbonate peak.
321 At 60 °C (Figure 12), the stable phases differ significantly from those at 20 °C and 38 °C. The
322 ettringite peak is not observed because this phase is not stable at 60 °C [33]. The 100C sample
323 does show small peaks of hemicarbonate. The main diffraction peak observed for the 60C40D
324 sample is hydrotalcite, already present from 90 days of hydration on, and no monocarbonate is
325 detected. When 5%wt of metakaolin is added (60C35D5M), hemicarbonate is observed in
326 addition to the hydrotalcite after 90 days, but it transforms to hydrotalcite at later ages. With
327 metakaolin additions of 10%wt, monosulphate is detected together with monocarbonate, and
328 only a small hydrotalcite shoulder is observed after 1 year of curing. At higher metakaolin levels,

329 the monocarbonate is replaced by hemicarbonate. Again, this could be due to the additional
330 metakaolin, which provides more Al_2O_3 and reduces the CO_2/Al_2O_3 ratio [32].
331 Clear peaks of hydrotalcite can only be observed with XRD in samples containing dolomite with a
332 relatively low metakaolin content (<10%wt) cured at elevated temperatures (38 °C and especially
333 at 60 °C). When metakaolin additions are high, or when the samples are cued at 20 °C, hydrotalcite
334 was not observable as a peak but as a small shoulder at the low-angle side of the monocarbonate
335 peak.
336
337 The hydrotalcite observed using XRD originates from the dolomite reaction because analogue
338 samples containing limestone do not show hydrotalcite-related reflections even after curing for 1
339 year at 60 °C (Figure 13). The XRD plots in Figure 13 also do not show clear peaks of carbonate
340 AFm phases. This can either be explained by the fact that they are not stable, or that they are less
341 crystalline and therefore X-ray amorphous at such a high curing temperature.
342
343 Figure 14 shows the XRD-patterns for 60C20D20M samples prepared with the two different w/b
344 ratios. No hydrotalcite peaks were detected after 400 days of curing. This is in line with the
345 observations from SEM-EDS that a high w/b ratio was not able to enhance the dolomite reaction
346 of the 60C20D20M sample.
347
348 **3.2.3 TGA**
349
350 Figure 15 shows the DTG curves for samples 60C40D and 60C40L after curing for 1 year at 60 °C.
351 Based on the XRD and SEM analysis, we would expect a considerable amount of hydrotalcite to
352 have formed in 60C40D, but not in 60C40L. Hydrotalcite is reported to decompose in two steps
353 during a TGA measurement. The first weight loss related to hydrotalcite is observed at approx.
354 220 °C and the second weight loss at approx. 380 °C [21]. These two steps appear as peaks in the
355 DTG curves for the sample 60C40D and are shown in Figure 15. Moreover, it should be noted that

small peaks of AFm phases are detected in the DTG curves of the samples 100C and 60C40L. This confirms the findings with XRD, which indicated that the AFm phases in the samples cured at 60 °C are probably X-ray amorphous.

In Figure 16 the differences between the samples containing dolomite and limestone with regard to the summed hydrotalcite weight losses of both of its weight loss steps are plotted for the various compositions and curing temperatures. This is done to eliminate the potential impact from Portland cement. The Portland cement used contains significant amounts of magnesium (Table 1) and might also cause a weight loss in the temperature range of hydrotalcite decomposition, as shown in Figure 15 for the sample 60C40L. So, positive values indicate a higher weight loss in the hydrotalcite temperature range for samples containing dolomite than for those containing limestone. It should be noted that, due to the probability of overlapping weight losses in this temperature interval, the signal recorded might not exclusively originate from the decomposition of hydrotalcite. Taking into account an estimated error of 0.1%wt, it seems that considerable hydrotalcite formation starts quite late. As Figure 16 shows, there are no significant differences in the weight losses after 28 days and only a small difference after 90 days between samples containing dolomite and limestone. Only in the 208-day-old and the 360-day-old samples are significantly higher hydrotalcite weight losses detected for samples containing dolomite than for those containing limestone when cured at 60 °C. The highest value is shown by the sample 60C40D after 360 days of hydration. With the addition of metakaolin, the hydrotalcite weight losses decrease. These observed trends are in good agreement with the XRD results, where the formation of hydrotalcite can be detected after 90 days and especially after 208 and 360 days in samples with low metakaolin additions (< 10%wt), with the sample 60C40D showing the highest hydrotalcite peaks when cured at elevated temperatures (especially 60 °C).

Portlandite dehydrates between approx. 400 °C and 550 °C, and a clear weight loss can be observed in the DTG signal (Figure 15). Figure 17 shows the portlandite content of sample mixes containing various amounts of dolomite or limestone at the temperatures investigated. A clear reduction can be seen in portlandite with increasing metakaolin content. This is due to the

pozzolanic reaction of metakaolin. This reaction is enhanced when the curing temperature is increased. It should be noted that the portlandite content for the samples containing 15%wt and 20%wt of metakaolin is similar. This indicates that at metakaolin contents >10%wt, its reaction is limited.

Figure 18 plots the differences in the portlandite content between the samples containing dolomite and limestone (estimated error: 0.5%wt). Therefore, negative values indicate a lower portlandite content in samples containing dolomite than in those containing limestone. These differences are only visible for compositions where there are also differences in the hydrotalcite weight loss. The sample 60C40D shows significantly lower portlandite content than its limestone equivalent (60C40L) after 208 and 360 days, when cured at 60 °C. This observation indicates that portlandite is consumed during the formation of hydrotalcite from dolomite. This is in-line with descriptions of the reaction of dolomite in the literature [14,15,16], where the dolomite reaction requires the presence of portlandite.

Figure 19 shows the portlandite content of the samples 60C20D20M with a w/b ratio of 0.45 and 0.93, both cured at 20 °C, 38 °C and 60 °C for 400 days. In samples with the low w/b ratio, the portlandite content is consumed almost completely when cured at 60 °C, but at lower curing temperatures more portlandite remains. In the samples with the high w/b ratio, the portlandite is completely consumed at all curing temperatures. These results indicate that in the range tested, increasing the w/b ratio enhances the metakaolin reaction.

3.3 MIP

The threshold pore entry diameter and the porosity were estimated from the intrusion curves of the first intrusion cycle of the mercury and are plotted for the various compositions in Figure 20. Figure 20 a) shows the results for samples cured at 38 °C for 208 days, Figure 20 b) for samples cured at 60 °C for 208 days and in Figure 20 c) for the samples cured at 60 °C for 360 days. The

409 precision of the MIP results was estimated to 20% for the threshold diameter and 1.5% for the
410 porosity according to [34].
411 Generally, the samples containing dolomite or limestone show similar results. In Figure 20 b)
412 however, there is a significant difference between the samples containing either 5%wt of dolomite
413 or limestone, which were cured at 60 °C. In order to elucidate whether this is an effect of hydration
414 or sample preparation, a set of samples cured as well at 60 °C but for 360 days was investigated
415 as well (Figure 20 c). After 360 days the samples containing dolomite or limestone show again
416 very similar results. This indicates that the differences observed in Figure 20 b) are due to sample
417 preparation effects.
418 If we compare the two curing temperatures (Figure 20 a & b), a coarsening effect can be observed
419 at the higher curing temperature. This effect is related to the transformation of ettringite to
420 monosulphate above 48 °C and a densification of the C-S-H phase at elevated temperatures, both
421 resulting in a coarsening of the pore structure [33]. Moreover, an increase in the porosity and the
422 threshold diameter can be observed if we compare the reference 100C with the sample containing
423 40%wt of dolomite or limestone at both temperatures. This is in agreement with previous findings
424 [20]. This coarsening effect of added carbonates can be counteracted by the addition of
425 metakaolin, which reduces the threshold diameter as described in the literature [9]. At high
426 metakaolin additions, the threshold pore entry diameter decreases down to values of approx.
427 0.04 µm for both curing temperatures. The addition of 5%wt of metakaolin decreases also the
428 porosity compared to the samples only containing dolomite or limestone. However, with additions
429 greater than 5%wt metakaolin, there is no further reduction in the porosity.
430
431 Figure 21 shows the threshold pore entry diameter and porosity of the samples prepared with the
432 different w/b ratio of 0.93 or 0.45 cured at 38 °C or 60 °C for 400 days. The threshold diameter
433 and the porosity are increased for the samples prepared with the high w/b ratio compared to the
434 samples with the low w/b ratio. This coarsening effect of the increased w/b ratio is expected and
435 in good agreement with the microstructural changes between samples with a high or low w/b

ratio as observed in the BSE images (Figure 7). While the threshold diameter is increased for the samples cured at 60 °C compared to 38 °C for both w/b ratios, the porosity is rather similar for the samples cured at 60 °C or 38 °C for both w/b ratios and no considerable increase in porosity can be observed.

3.4 Well-hydrated samples exposed to additional water and or portlandite

Figure 22 shows the DTG curves of the sample 60C20D20M+H_2O, which was exposed to 30%wt additional water after 28 and 90 days of exposure at 60 °C, compared to the same sample prior exposure. The sample 60C20D20M+H_2O was used as a reference to the sample 60C20D20M+CH, which was exposed to additional 30%wt water and 30%wt portlandite. As the reference samples after 28 and 90 days of exposure show almost completely the same curves as the sample prior exposure, we assume that they were stable during the whole exposure time. Consequently, any phase changes observed in the sample 60C20D20M+CH are due to the addition of portlandite and not due to the addition of water.

Figure 23 shows the DTG curves of the sample 60C20D20M+CH cured for 28 and 90 days at 60 °C compared to the sample prior exposure. At low temperatures (40–300 ° C), the samples exposed to portlandite are shifted upwards compared to the sample prior exposure and show as well a decreased peak in the temperature range of the dolomite decomposition. This can be explained by the dilution effect of the hydrates and the dolomite in the samples where 30%wt of portlandite was added. Because of this addition, these samples also show a clear peak in the temperature interval of the portlandite decomposition. The two peaks related to the decomposition of hydrotalcite increased with exposure time in the samples exposed to portlandite compared to the sample prior exposure. This indicates the formation of hydrotalcite in these samples. The samples exposed to portlandite also show an additional peak in the AFm-temperature region, probably due to the formation of monosulphate. This peak seems to decrease with the exposure time. The

increase in the hydrotalcite peak simultaneously with the decrease in the monosulphate peak indicates that due to the reaction of dolomite over time in the samples exposed to portlandite, the monosulphate transforms to hydrotalcite as it is thermodynamically more stable [35].

Figure 24 shows the XRD-patterns of the samples 60C20D20M+CH and 60C20D20M+H_2O after 90 days of exposure compared to the sample prior exposure. While the sample prior exposure and the reference sample show the same phase assemblage, the sample 60C20D20M+CH shows additional peaks. In this sample, besides the portlandite peak due to the exposure, clear peaks of monosulphate and hydrotalcite are visible. These results are in good correlation with the observations made in the DTG curves of these samples.

4 DISCUSSION

The results of this study show that dolomite can react significantly when added to Portland cement, depending on the curing age, temperature and the metakaolin content of the samples. The reaction products and the limitations of this reaction are discussed in the following.

4.1 What are the products of the dolomite reaction?

The elemental maps obtained from SEM-EDS analysis show that when dolomite reacts magnesium does not move outside the former grain boundary of the dolomite, probably due to a limited mobility of magnesium in high pH environments [1]. So, the magnesium-containing reaction products of dolomite form a reaction rim within the former dolomite grain boundaries. The products in the reaction rim contain magnesium, aluminium and show a higher oxygen content. The high oxygen content indicates that the reaction products are hydrates. No silicon can be found in the rims and the calcium content is less than in the original dolomite grain. The lack of silicon in the rims excludes M-S-H as a reaction product.

EDS point analysis of the reaction rims indicates the presence of hydrotalcite, with a Mg/Al ratio of approx. 2.4–3.2 depending on the metakaolin content of the cement. The formation of hydrotalcite was confirmed by XRD, where peaks of hydrotalcite could be found in samples where significant amounts of dolomite have reacted. XRD did not detect clear peaks of brucite in any samples. TGA analysis seems to indicate that the weight losses in the temperature range of hydrotalcite correlate to the amount of dolomite reacted.

We conclude that hydrotalcite is the only magnesium-containing product of the dolomite reaction and it forms in reaction rims within the former dolomite grains in samples cured at elevated temperatures (60 °C).

TGA and XRD also showed that the addition of dolomite results in the formation of carbonate AFm phases and therefore ettringite stabilization. This means that the dolomite delivers carbonates to the system, which can form carbonate AFm phases. This is only observable in samples where ettringite is stable, hence in samples cured at 20 °C or 38 °C. Calcite might also be formed due to the reaction of dolomite. XRD detected calcite in the samples, but we could not confirm whether this calcite was formed during the dedolomitization reaction. This is because the dolomite used already contains approx. 6%wt of calcite, which might partially also participate in the formation of carbonate AFm phases. SEM-EDS cannot differentiate between portlandite and calcite, so the potential replacement of portlandite with calcite during the dolomite reaction cannot be identified.

These findings are in agreement with Zajac et al., who showed that in the presence of other ions dolomite reaction results in the formation of hydrotalcite and carbonate AFm phases, which lead to the stabilization of ettringite [17].

4.2 What limits the hydrotalcite formation?

As described above, hydrotalcite forms slowly over time in samples containing dolomite which have been cured at 60 °C, if they contain less than 10%wt of metakaolin.

To elucidate the possible limitations of the hydrotalcite formation, Equation (1) gives an idealized reaction based on the observations in this study. In this reaction, dolomite reacts with a source of aluminium, here given as $Al(OH)_3$, and portlandite to form hydrotalcite and calcite. This reaction inside the reaction rims around the dolomite grains is illustrated in Figure 25. The calcite formed might then precipitate in the matrix or in finely intermixed with the C-S-H in the rim, which indicates the original grain boundary of the dolomite. It might also partially contribute to the formation of hemi- or monocarbonate. The hydrotalcite formation could be chemically limited by any of the reactants given in Equation (1). Taking into account the refinement of the pore structure due to the metakaolin addition, there might be a physical limitation as well.

$$6CaMg(CO_3)_2 + 2Al(OH)_3 + 6Ca(OH)_2 + 9H_2O \rightarrow Mg_6Al_2(OH)_{18}{\cdot}3(H_2O) + 12CaCO_3 \text{ (Hc / Mc)} \quad (1)$$

In the following, we discuss the various possible limitations in detail:

4.2.1 Pore space as a physical limitation

The MIP results for the samples cured at 60 °C (Figure 20) show that while the porosity is not decreased, the threshold diameter is significantly refined with the addition of metakaolin. The threshold pore diameter, which is an important parameter for transport in the pore system [36], is reduced from 0.4 µm, for the samples only containing dolomite but no metakaolin, to 0.04 µm, for the samples with the highest metakaolin content. Durdzinski, 2016 reported the refinement of the pore structure due to the additions of fine and reactive SCMs to be the major factor for a decreased degree of reaction. This observation was explained with the restricted transport and the hindered crystallization in fine pores compared to coarse pores [34]. This is in agreement with the TGA results, which show a limited further reaction of metakaolin for additions of metakaolin higher than 10%wt (see Figure 17). This possible hindrance of further reactions in dense systems has been reported for metakaolin or other SCMs and UHPC previously [34,37,38].

The MIP results also show that curing at 60 °C considerably coarsens the pore structure. So, in addition to the higher reactivity of dolomite at 60 °C than at 38 °C reported before [14–17], the coarser pore structure might also facilitate the ongoing reactions due to the facilitation of transport and crystallization.

To elucidate the effect of the pore space, we prepared samples with high amounts of metakaolin (20%wt) and a high w/b ratio (0.93). The XRD plots (Figure 14) show that, despite the coarse pore structure of these samples, no hydrotalcite was formed, and the BSE images also showed that the dolomite did not react (Figure 7). We, therefore, conclude that the limited pore space in metakaolin-rich samples does not act as a major limitation on the dolomite reaction in the investigated systems.

4.2.2 Aluminium availability

Figure 25 shows a schematic illustration of the hydrotalcite formation inside the former dolomite grain boundary including the necessary transport of ions. Aluminium is needed for hydrotalcite to form, see Equation (1) and Figure 25. The addition of metakaolin to the system provides additional aluminium. Besides the formation of hydrotalcite, this additional aluminium can result in the increased formation of AFm phases shown in XRD (see Figure 11), and the uptake of aluminium in the C-S-H shown in SEM-EDS (see Figure 9). Hydrotalcite will win the competition for the aluminium over AFm phases because it is thermodynamically more stable [35], but we cannot reach a conclusion on the competition with the Al-uptake in the C-S-H, due to limited thermodynamic data. When comparing the Al/Si ratios of the C-S-H (Figure 9) to the Al/Si ratios reported in the literature, we can see that for low metakaolin additions (5%wt), our values are somewhat lower, and for high metakaolin additions, they are higher than reported in the literature [12]. Our data does therefore not fit the proposed fitting equation by Dai et al. [12]. This might be explained by the formation of hydrotalcite in the samples containing lower amounts of

568 metakaolin, which was shown to reduce the aluminium content of the C-S-H [17]. If aluminium
569 does act as a limiting factor in the hydrotalcite formation reaction, the addition of aluminium
570 through the addition of metakaolin should increase the amount of hydrotalcite formed. A similar
571 effect of additional aluminium has been reported on the formation of carbonate AFm phases [5–
572 8].
573
574 However, it was shown that with the addition of 5%wt of metakaolin there is no increase in the
575 amount of hydrotalcite formed. Consequently, we can conclude that any possible positive effect
576 from the additional aluminium is unable to compensate for the negative effects of metakaolin
577 addition on hydrotalcite formation. We, therefore, conclude that the availability of aluminium
578 does not act as a major limitation on the dolomite reaction in the investigated systems.
579

580 ### 4.2.3 Dolomite dissolution

581
582 Hydrotalcite is a magnesium-containing hydrate. The availability of magnesium and hence the
583 dissolution of dolomite are required for hydrotalcite to form. This is illustrated in Figure 25, where
584 the formation of a reaction rims, in which the magnesium from the dolomite dissolution is
585 indicated. The dissolution of dolomite has been reported to be slow. However, it was shown to be
586 accelerated by increasing the curing temperature from 25 °C to 60 °C [14–17]. This is in good
587 agreement with our results, as we observed an increased reaction degree of dolomite when cured
588 at 60 °C compared to 38 °C or 20 °C. In samples cured at 60 °C with low or no metakaolin content,
589 QXRD showed that significant amounts of dolomite have reacted after 360 days of curing. This
590 also explains the observed hydrotalcite formation only in samples cured at elevated temperatures.
591 However, only samples with low or no metakaolin addition show significant dolomite reaction
592 and hydrotalcite formation when cured at 60 °C. This indicates that the dissolution of dolomite is
593 additionally limited by another factor besides temperature.
594

595 Equation 2 gives portlandite as one of the reactants for the hydrotalcite formation. Even though
596 hydrotalcite ($Mg_6Al_2(OH)_{18}{\cdot}3(H_2O)$) does not contain calcium, the formation of hydrotalcite is
597 associated with the consumption of portlandite (Figure 18) to form calcite (as indicated in Figure
598 25), similarly to the reported dedolomitization reaction, where brucite is formed [14–16]. To
599 illustrate the consumption of portlandite due to the reaction of dolomite, we plotted the difference
600 in portlandite weight loss between samples containing dolomite and samples containing
601 limestone in Figure 18. Samples containing dolomite show significantly lower portlandite content
602 than samples containing limestone. This is especially visible at the elevated curing temperatures
603 and low metakaolin additions, which cause significant dolomite reaction (Figure 2) and
604 consequent hydrotalcite formation (Figure 16). The need for portlandite by the reaction of
605 dolomite can be explained by the difference between dolomite, which contains 2 mol CO_3^{2-} per
606 mol dolomite, and calcite, which contains 1 mol of CO_3^{2-} per mol of calcite. Therefore, to make the
607 magnesium available for reaction to hydrotalcite, calcium is needed to compensate for the other
608 carbonate ion from the dolomite, similar as for the dedolomitization reaction in which brucite is
609 formed. The experimental techniques in this study did not allow the differentiation between
610 carbonate-containing hydrotalcite and a carbonate-free hydrotalcite. However, as long as the
611 hydrotalcite contains less than 1 mol of CO_3^{2-} per mol of hydrotalcite [19,39–42], additional
612 calcium is needed in the reaction to compensate for the rest of the carbonate ions. This is also
613 indicated in Figure 25 by the transport of CO_3^{2-} ions out of the reaction rims.
614
615 The portlandite availability varies with the metakaolin content. A higher metakaolin content leads
616 to an increased consumption of portlandite due to its pozzolanic reaction, as TGA shows in Figure
617 17. As portlandite is consumed in the reaction of dolomite and the formation of hydrotalcite, and
618 it is, therefore, a possible limitation to this reaction in samples where most or all of the portlandite
619 has already been consumed in the fast pozzolanic reaction of the metakaolin.
620

It was shown from the results of the samples prepared with the various w/b ratios that the higher w/b ratio enhances not only the Portland cement reaction but also the metakaolin reaction. This led to the complete consumption of the portlandite in the system (Figure 19). Because metakaolin addition refines the pore structure and consumes Portlandite at the same time, these two factors are not completely distinguishable. Because of this, a part of the samples 60C20D20M cured at 60 °C for 1 year and 9 months, were exposed to 30%wt portlandite and or 30%wt of additional water for up to 90 days. While the samples, which were exposed only to water, did not change during exposure, the samples exposed to water and portlandite showed the formation of hydrotalcite over time. It can be concluded that in samples, which contain high amounts of metakaolin (20%wt) and therefore have a refined pore structure, the formation of hydrotalcite can be observed as long as sufficient portlandite is available. This confirms the lack of Portlandite as a limiting factor due to the correlation between portlandite consumption and hydrotalcite formation, independently of the pore structure. The refined pore structure in the samples containing high amounts of metakaolin might slow down the reactions but is not inhibiting the formation of hydrotalcite.

5 CONCLUSION

Cement pastes, in which 40%wt of Portland cement clinker was replaced by either dolomite or limestone in combination with 0–20%wt metakaolin, were investigated with regard to their phase assemblage and microstructure. The samples were cured at 20 °C, 38 °C and 60 °C up to 360 days. Additionally, samples with a high w/b ratio (0.93) were prepared and investigated after 400 days of curing and parts of the samples containing 20%wt of metakaolin were exposed to additional portlandite and or water for up to 90 days. The following conclusions are made based on the investigations:

Within 360 days, significant amounts of the added dolomite react at low metakaolin additions (<10%) and an elevated curing temperature (60 °C). As a result of the reaction, magnesium and

carbonates are supplied to the system. The carbonates originating from the dolomite stabilize ettringite due to the formation of carbonate AFm phases. During the dolomite reaction, portlandite is consumed and hydrotalcite is formed. Hydrotalcite ($Mg_6Al_2(OH)_{18}{\cdot}3(H_2O)$) is the only magnesium-containing reaction product from the dolomite reaction. Neither M-S-H nor brucite were detected in any samples investigated.

To check whether additional aluminium results in additional hydrotalcite formation, up to 20%wt of metakaolin was added to the system. However, instead of promoting the hydrotalcite formation, the addition of more than 5%wt metakaolin inhibited the dolomite reaction and therefore also the hydrotalcite formation. Thus, aluminium availability is no major limitation for hydrotalcite formation.

The addition of metakaolin influenced the system in more ways than solely providing aluminium. It also consumes portlandite during its pozzolanic reaction and simultaneously refines the pore structure. From the results of the samples containing 20%wt metakaolin which were exposed to additional metakaolin and or water, we can conclude that the pore structure refinement is not inhibiting the formation of hydrotalcite, but might slow reactions down. By investigating the samples with the high w/b ratios, the absence of portlandite in high-metakaolin samples could be confirmed to inhibit the reaction of dolomite and the formation of hydrotalcite independently of any impact from the pore structure.

6 ACKNOWLEDGEMENTS

The authors would like to thank the industrial PhD programme of the Norwegian Research Council (Project: 241637) and the Heidelberg Technology Center for their financial support.

We are also very grateful for the helpful discussion with Christopher Stabler on the dolomite quantification by XRD Rietveld analysis.

7 References

[1] K.L. Scrivener, M.J. Vanderley, E.M. Gartner, Eco-efficient cements: Potential, economically viable solutions for a low-CO_2 cement-based materials industry, United Nations Environment Program – Building and Climate Initiative (UNEP-SBCI), Paris, 2016.

[2] EN 197-1, Cement, Part I: Composition, specifications and conformity criteria for common cements, European Committee for Standardization, Brussels, 2011.

[3] T. Matschei, B. Lothenbach, F.P. Glasser, The role of calcium carbonate in cement hydration, Cem Concr Res 37 (2007) 551–558.

[4] B. Lothenbach, G. Le Saout, E. Gallucci, K.L. Scrivener, Influence of limestone on the hydration of Portland cements, Cem Concr Res 38 (2008) 848–860.

[5] K. De Weerdt, K.O. Kjellsen, E. Sellevold, H. Justnes, Synergy between fly ash and limestone powder in ternary cements, Cement and Concrete Composites 33 (2011) 30–38.

[6] M. Antoni, J. Rossen, F. Martirena, K.L. Scrivener, Cement substitution by a combination of metakaolin and limestone, Cem Concr Res 42 (2012) 1579–1589.

[7] D. Nied, C. Stabler, M. Zajac, Assessing the synergistic effect of limestone and metakaolin, in: K.L. Scrivener, A. Favier (Eds.), Calcined Clays for Sustainable Concrete: Proceedings of the 1st International Conference on Calcined Clays for Sustainable Concrete, 2015, pp. 245–251.

[8] G. Puerta-Falla, M. Balonis, G. Le Saout, N. Neithalath, G. Sant, The Influence of Metakaolin on Limestone Reactivity in Cementitious Materials, in: K.L. Scrivener, A. Favier (Eds.), Calcined Clays for Sustainable Concrete: Proceedings of the 1st International Conference on Calcined Clays for Sustainable Concrete, 2015, pp. 11–19.

[9] T.R. Jones, Metakaolin as a pozzolanic addition to concrete, in: J. Bensted, P. Barnes (Eds.), Structure and Performance of cements, 2nd ed., Taylor & Francis, New York, 2002, pp. 372–398.

[10] E. L'Hôpital, B. Lothenbach, G. Le Saout, D.A. Kulik, K.L. Scrivener, Incorporation of aluminium in calcium-silicate-hydrates, Cem Concr Res 75 (2015) 91–103.

[11] I.G. Richardson, The nature of C-S-H in hardened cements, Cem Concr Res 29 (1999) 1131–1147.

[12] Z. Dai, T.T. Tran, J. Skibsted, H. Jennings, Aluminum Incorporation in the C-S-H Phase of White Portland Cement-Metakaolin Blends Studied by ^{27}Al and ^{29}Si MAS NMR Spectroscopy, J. Am. Ceram. Soc. 97 (2014) 2662–2671.

[13] S. Schöne, W. Dienemann, E. Wagner, Portland Dolomite Cements as Alternative to Portland Limestone Cements, in: Proceedings of the 13th International Congress on the Chemistry of Cement, Madrid, 2011.

[14] S. Galí, C. Ayora, P. Alfonso, E. Tauler, M. Labrador, Kinetics of dolomite-portlandite reaction: Application to Portland cement concrete, Cem Concr Res 31 (2001) 933–939.

[15] E. Garcia, P. Alfonso, M. Labrador, S. Galí, Dedolomitization in different alkaline media: Application to Portland cement paste., Cem Concr Res 33 (2003) 1443–1448.

[16] X. Zhang, F.P. Glasser, K.L. Scrivener, Reaction kinetics of dolomite and portlandite, Cem Concr Res 66 (2014) 11–18.

[17] M. Zajac, S.K. Bremseth, M. Whitehead, M. Ben Haha, Effect of $CaMg(CO_3)_2$ on hydrate assemblages and mechanical properties of hydrated cement pastes at 40 °C and 60 °C, Cem Concr Res 65 (2014) 21–29.

[18] M. Zajac, W. Dienemann, G. Bolte, Comparative experimental and virtual investigations of the influence of calcium and magnesium carbonates on reacting cement, in: Proceedings of the 13th International Congress on the Chemistry of Cement, Madrid, 2011.

[19] R.J. Myers, B. Lothenbach, S.A. Bernal, J.L. Provis, Thermodynamic modelling of alkali-activated slag cements, Applied Geochemistry 61 (2015) 233–247.

[20] J. Xu, D. Lu, Zhang S., K. Ling, Z. Xu, Pore Structures of Mortars with Dolomite and Limestone Powders Cured at Various Temperatures, Journal of the Chinese Ceramic Society 45 (2017) 268–273.

[21] B. Lothenbach, P. Durdzinski, K. De Weerdt, Thermogravimetric Analysis, in: K.L. Scrivener, R. Snellings, B. Lothenbach (Eds.), A Practical Guide to Microstructural Analysis of Cementitious Materials, CRC Press Taylor & Francis Group, Boca Raton, 2015, pp. 177–211.

[22] B.H. O'Connor, M.D. Raven, Application of the Rietveld Refinement Procedure in Assaying Powdered Mixtures, Powder Diffr. 3 (1988) 2–6.

[23] D. Jansen, F. Goetz-Neunhoeffer, C. Stabler, J. Neubauer, A remastered external standard method applied to the quantification of early OPC hydration, Cem Concr Res 41 (2011) 602–608.

[24] S.T. Bergold, F. Goetz-Neunhoeffer, J. Neubauer, Quantitative analysis of C–S–H in hydrating alite pastes by in-situ XRD, Cem Concr Res 53 (2013) 119–126.

[25] M.M. Canut, M.R. Geiker, Impact of curing on the porosity development of cement pastes with and without slag, in: Proceedings of the 13th International Congress on the Chemistry of Cement, Madrid, 2011.

[26] M. Ben Haha, B. Lothenbach, G. Le Saout, F. Winnefeld, Influence of slag chemistry on the hydration of alkali-activated blast-furnace slag – Part I: Effect of MgO, Cem Concr Res 41 (2011) 955–963.

[27] S. Adu-Amankwah, L. Black, M. Zajac, The effect of sulphates on limestone containing composite cements, in: University of Aberdeen (Ed.), 35th Cement and Concrete Science Conference, 2015.

[28] G. Fornasari, R. Glöckler, M. Livi, A. Vaccari, Role of the Mg/Al atomic ratio in hydrotalcite-based catalysts for NOx storage/reduction, Applied Clay Science 29 (2005) 258–266.

[29] S.-D. Wang, Alkali-activated slag: hydration process and development of microstructure, Advances in Cement Research 12 (2000) 163–172.

[30] S.-D. Wang, K.L. Scrivener, Hydration products of alkali activated slag cement, Cem Concr Res 25 (1995) 561–571.

[31] R. Allmann, H.P. Jespen, Die Struktur des Hydrotalkitts, Neues Jahrbuch für Mineralogie (Monatshefte) (1969) 544–551.

[32] T. Matschei, B. Lothenbach, F.P. Glasser, The AFm phase in Portland cement, Cem Concr Res 37 (2007) 118–130.

[33] B. Lothenbach, T. Matschei, G. Möschner, F.P. Glasser, Thermodynamic modelling of the effect of temperature on the hydration and porosity of Portland cement, Cem Concr Res 38 (2008) 1–18.

[34] P. Durdzinski, Hydration of multi-component cements containing cement clinker, slag, calcareous fly ash and limestone. Ph.D. Thesis, Lausanne, 2016.

[35] M. Zajac, M. Ben Haha, Hydration of limestone and dolomite cement, in: Proceedings of the 14th International Congress on the Chemistry of Cement, 2015.

[36] Z. Shi, M.R. Geiker, B. Lothenbach, K. de Weerdt, S.F. Garzón, K. Enemark-Rasmussen, J. Skibsted, Friedel's salt profiles from thermogravimetric analysis and thermodynamic modelling of Portland cement-based mortars exposed to sodium chloride solution, Cement and Concrete Composites 78 (2017) 73–83.

[37] W. Huang, H. Kazemi-Kamyab, W. Sun, K.L. Scrivener, Effect of cement substitution by limestone on the hydration and microstructural development of ultra-high performance concrete (UHPC), Cement and Concrete Composites 77 (2017) 86–101.

[38] W. Kunther, Z. Dai, J. Skibsted, Thermodynamic modeling of hydrated white Portland cement–metakaolin–limestone blends utilizing hydration kinetics from ^{29}Si MAS NMR spectroscopy, Cem Concr Res 86 (2016) 29–41.

[39] S. Miyata, The Syntheses of Hydrotalcite-Like Compounds and Their Structures and Physico-Chemical Properties I: The Systems Mg^{2+}-Al^{3+}-NO_3^-, Mg^{2+}-Al^{3+}-Cl^-, Mg^{2+}-Al^{3+}-ClO_4^-, Ni^{2+}-Al^{3+}-Cl^- and Zn^{2+}-Al^{3+}-Cl^-, Clays and Clay Minerals 23 (1975) 369–375.

[40] K. Rozov, U. Berner, C. Taviot-Gueho, F. Leroux, G. Renaudin, D. Kulik, L.W. Diamond, Synthesis and characterization of the LDH hydrotalcite–pyroaurite solid-solution series, Cement and Concrete Research 40 (2010) 1248–1254.

[41] K.B. Rozov, U. Berner, D.A. Kulik, L.W. Diamond, Solubility and thermodynamic properties of carbonate-bearing hydrotalcite–pyroaurite solid solutions with a 3:1 Mg/(Al+Fe) mole ratio, Clays Clay Miner. 59 (2011) 215–232.

[42] S.J. Mills, A.G. Christy, J.-M.R. Génin, T. Kameda, F. Colombo, Nomenclature of the hydrotalcite supergroup: Natural layered double hydroxides, Mineral. Mag. 76 (2012) 1289–1336.

8 TABLES

Table 1: XRF results [%wt] of the clinker, dolomite, limestone, metakaolin and gypsum used.

Oxide	Clinker	Dolomite	Limestone	Metakaolin	Gypsum
SiO_2	20.6	0.52	0.12	52.18	0.02
Al_2O_3	5.6	0.01	0.06	44.92	0.09
TiO_2	0.29	0.00	0.00	1.14	0.00
MnO	0.05	0.00	0.00	0.00	0.00
Fe_2O_3	3.12	0.04	0.03	0.62	0.00
CaO	63.26	31.52	55.12	0.12	32.66
MgO	2.66	20.14	0.41	0.04	0.06
K_2O	1.23	0.00	0.01	0.18	0.01
Na_2O	0.51	0.00	0.00	0.17	0.02
SO_3	1.37	0.00	0.02	0.14	46.47
P_2O_5	0.09	0.01	0.00	0.07	0.00
LOI	-	46.79	43.57	0.29	20.39
Sum (1050 °C)	**98.78**	**99.03**	**99.34**	**99.87**	**99.72**

Table 2: Mineral composition of the dolomite, limestone, metakaolin and gypsum, determined by Rietveld analysis [%wt]. Amounts given in *italics* are below the limits of quantification (1%wt). Due to the low crystallinity of mullite, its quantification is questionable.

Mineral name	Mineral formula	Dolomite	Limestone	Metakaolin	Gypsum
Calcite	$CaCO_3$	5.8	100	-	-
Dolomite	$CaMg(CO3)_2$	89.9	-	-	-
Gypsum	$CaSO_4{\cdot}2H_2O$	-	-	-	93.7
Bassanite	$CaSO_4{\cdot}0.5H_2O$	-	-	-	6.3
Anatase	TiO_2	-	-	*1.2*	-
Mullite	$Al_6Si_2O_{13}$	-	-	*6.1*	-
Muscovite	$KAl_2Si_3AlO_{10}(OH)_2$	-	-	*0.4*	-
Quartz	SiO_2	*0.4*	-	*0.7*	-
Amorphous content	-	3.9	-	91.6	-

Table 3: Mineralogical composition of the clinker used determined by Rietveld analysis [%wt]. Amounts given in italics are below or close to the limits of detection.

Mineral name	Formula	%wt
Alite	Ca_3SiO_5	59.5
Belite	Ca_2SiO_4	15.3
Aluminate	$Ca_3Al_2O_6$	8.8
Ferrite	$Ca_2(Al,Fe)_2O_5$	10.0
Periclase	MgO	1.5
Free Lime	CaO	0.9
Portlandite	$Ca(OH)_2$	*1.2*
Aphthitalite	$K_3Na(SO_4)_2$	*2.4*
Arcanite	K_2SO_4	*0.5*

797 Table 4: Overview of the experimental matrix, including the original composition, addition of water or portlandite, w/b
798 ratio and curing time of all samples. The times given in brackets represents the time of the samples exposed to
799 portlandite and or water. The sulphate content per gram of binder was set to 2.5%wt for all mixes [%wt]. It should be
800 noted that the dolomite contains approx. 90% of dolomite (see Table 2).

Name of the mix	**C** Portland cement clinker	**D** Dolomite	**L** Limestone	**M** Metakaolin	**Add. Water**	**Add. CH**	**w/b ratio**	**Curing time**
100C	100	-	-	-	-	-	0.45	28-360 d
60C40D	60	40	-	-	-	-	0.45	28-360 d
60C35D5M	60	35	-	5	-	-	0.45	28-360 d
60C30D10M	60	30	-	10	-	-	0.45	28-360 d
60C25D15M	60	25	-	15	-	-	0.45	28-360 d
60C20D20M	60	20	-	20	-	-	0.45	28-360 d
60C40L	60	-	40	-	-	-	0.45	28-360 d
60C35L5M	60	-	35	5	-	-	0.45	28-360 d
60C30L10M	60	-	30	10	-	-	0.45	28-360 d
60C25L15M	60	-	25	15	-	-	0.45	28-360 d
60C20L20M	60	-	20	20	-	-	0.45	28-360 d
60C20D20M w/b 0.45	60	20	-	20	-	-	0.45	400 d
60C20D20M w/b 0.93	60	20	-	20	-	-	0.93	400 d
60C20D20M + H_20	60	20	-	20	+30%	-	0.45	630 d (+ 28/90 d)
60C20D20M + CH	60	20	-	20	+30%	+30%	0.45	630 d (+ 28/90 d)

801

802

803 # 9 FIGURES

804

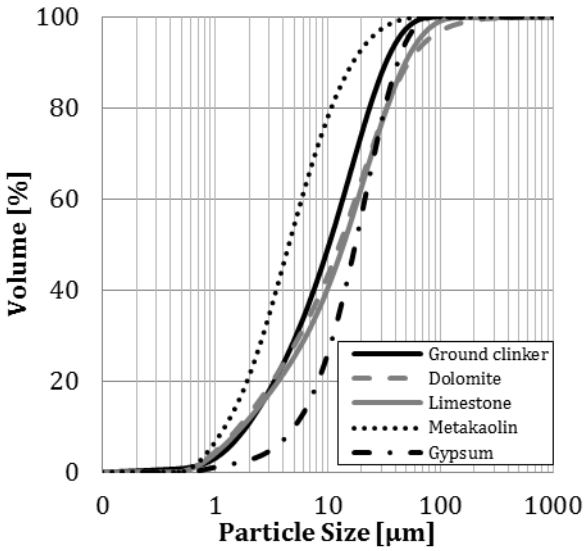

Figure 1: Particle size distributions of the materials used, determined by laser diffraction.

805

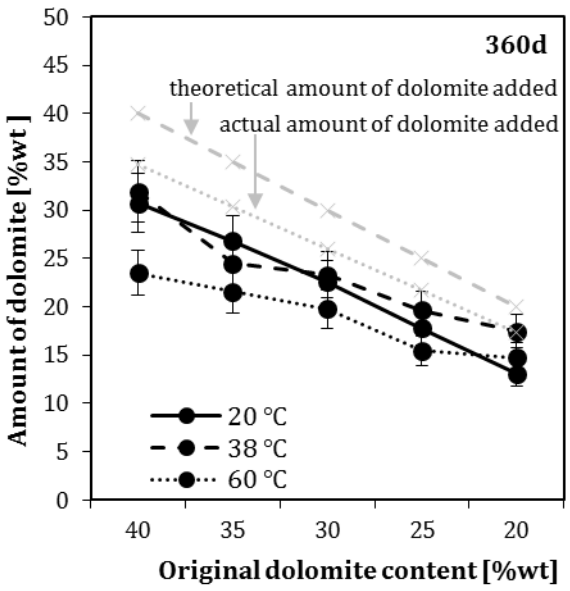

Figure 2: Amount of dolomite for the various compositions, in %wt compared to the original content of dolomite (theoretical and actual) for samples cured at 20 °C, 38 °C and 60 °C after 360 days.

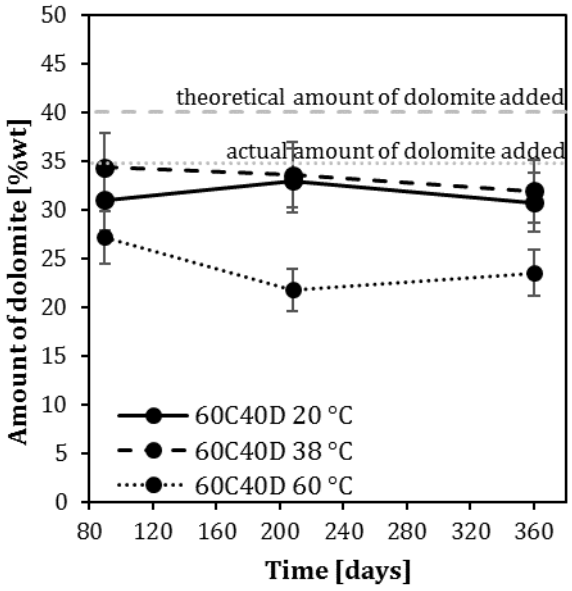

Figure 3: Amount of dolomite reacted over time, in %wt compared to the original content of dolomite (theoretical and actual) for the sample 60C40D cured at 20 °C, 38 °C and 60 °C.

806

60C40D 60 °C 360d

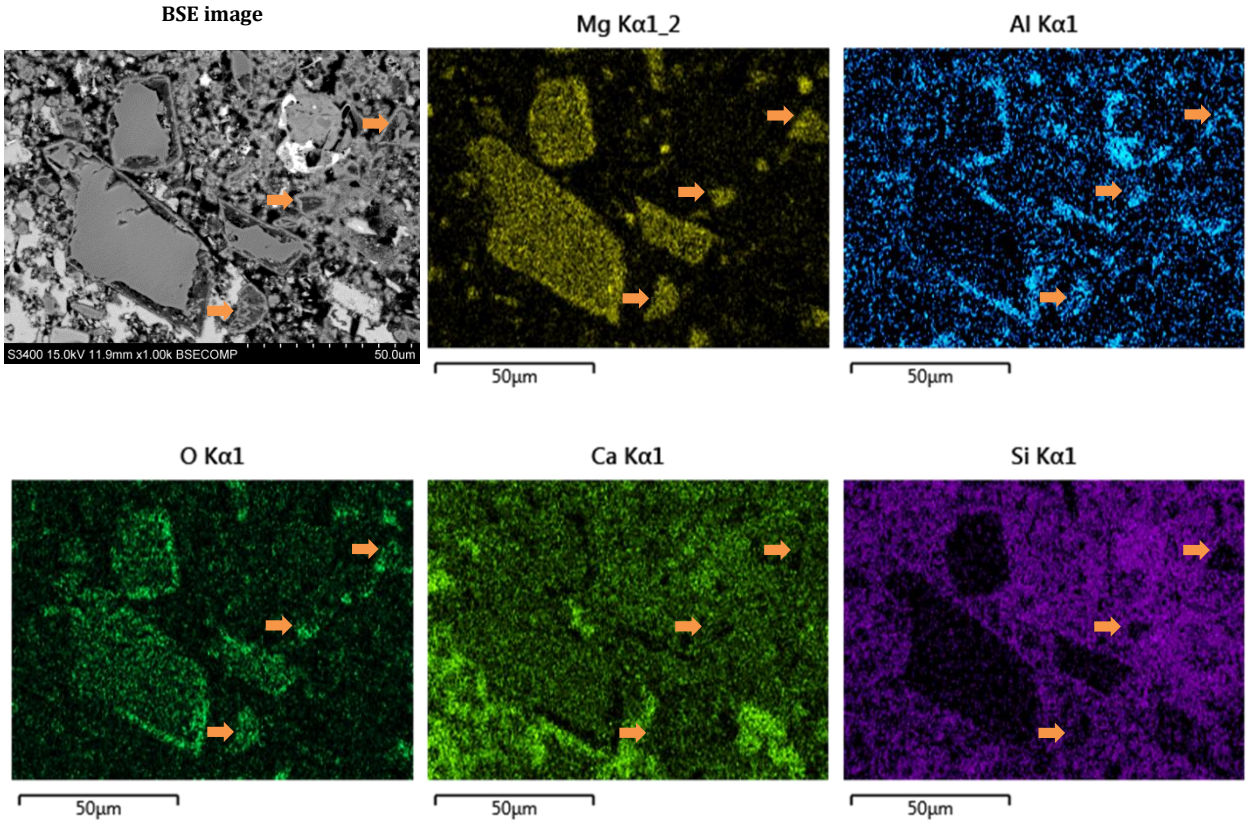

Figure 4: BSE image and elemental maps of magnesium, aluminium, oxygen, calcium and silicon for the sample 60C40D cured at 60 °C for 360 days. The arrows in the BSE image indicate small fully-reacted dolomite grains.

807

808

60C35D5M 60 °C 360d

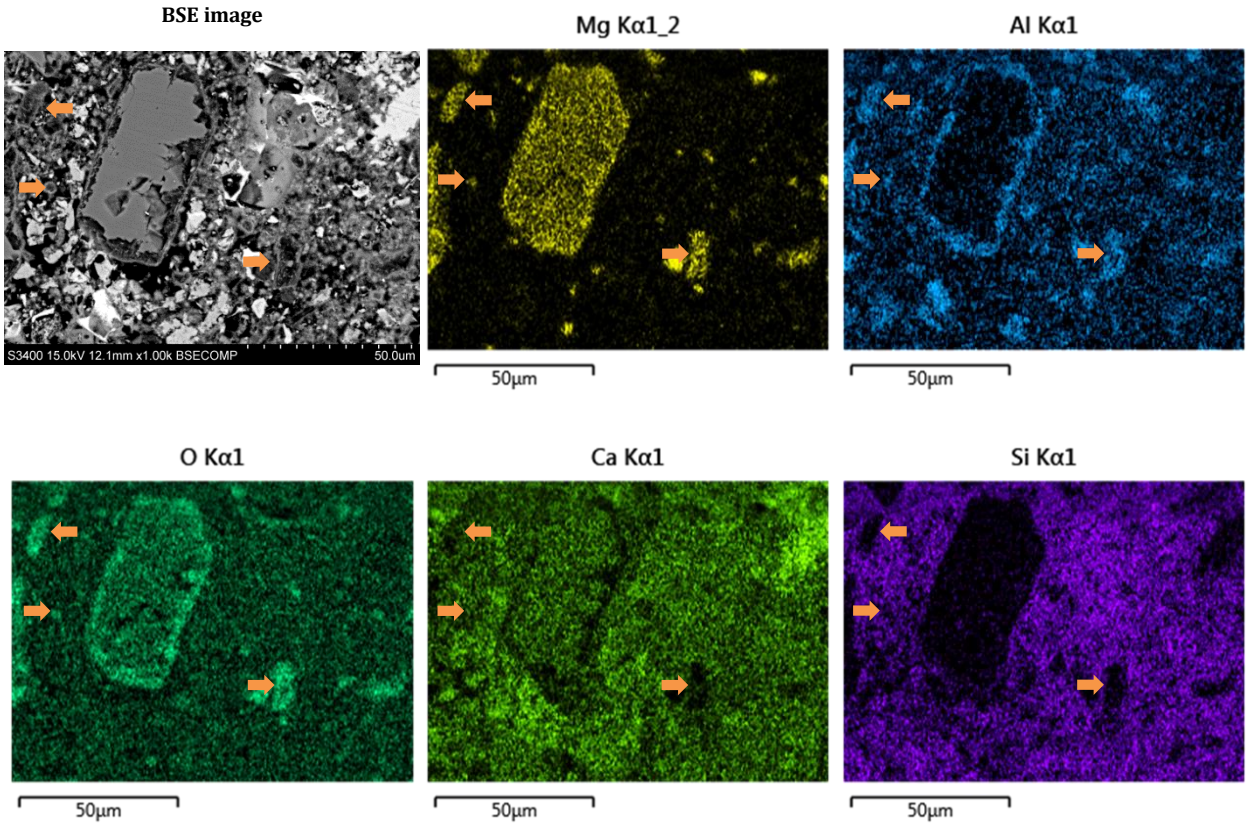

Figure 5: BSE image and elemental maps of magnesium, aluminium, oxygen, calcium and silicon for the sample 60C35D5M cured at 60 °C for 360 days. The arrows in the BSE image indicate small fully-reacted dolomite grains.

809

810

60C20D20M 60 °C 360d

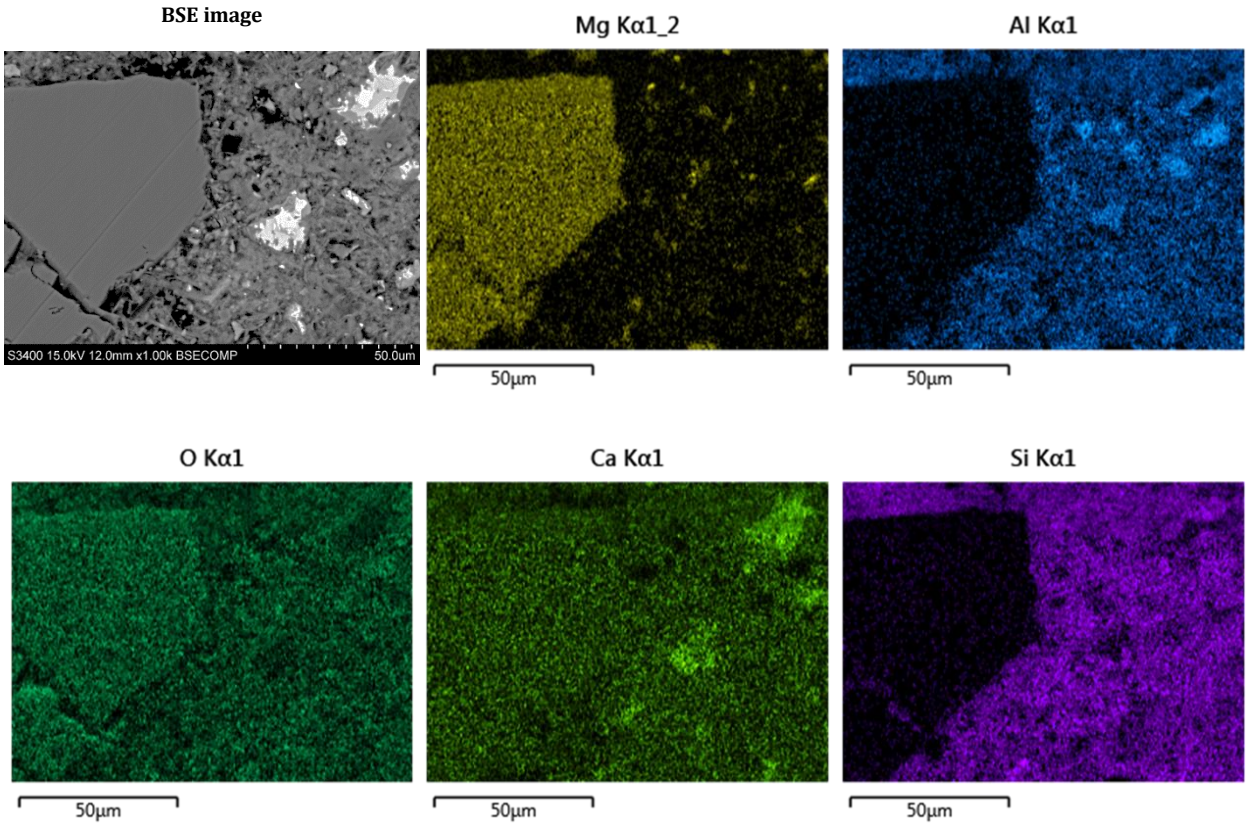

Figure 6: BSE image and elemental maps of magnesium, aluminium, oxygen, calcium and silicon for the sample 60C20D20M cured at 60 °C for 360 days.

811

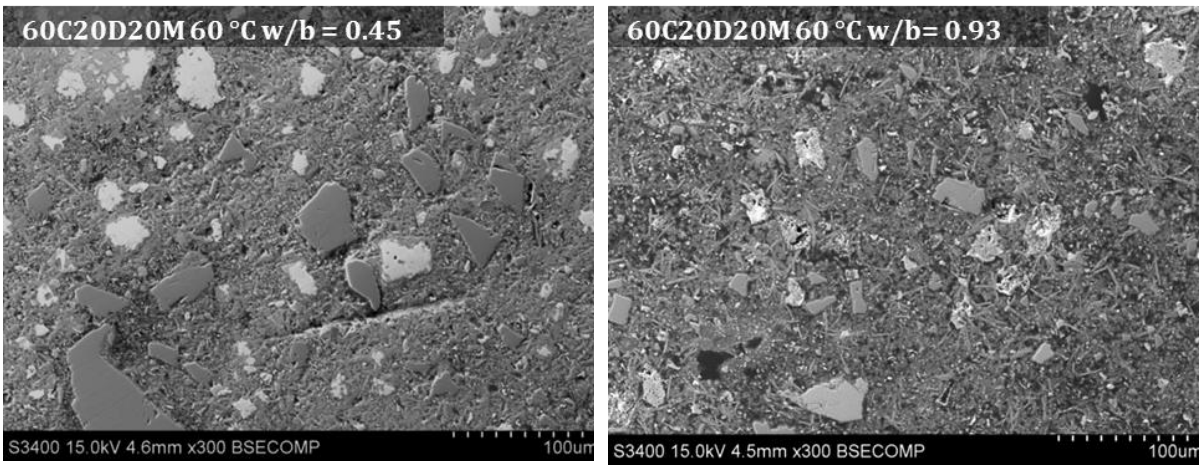

Figure 7: BSE images of the sample 60C20D20M with w/b ratios of 0.45 and 0.93 cured at 60 °C for 400 days.

812

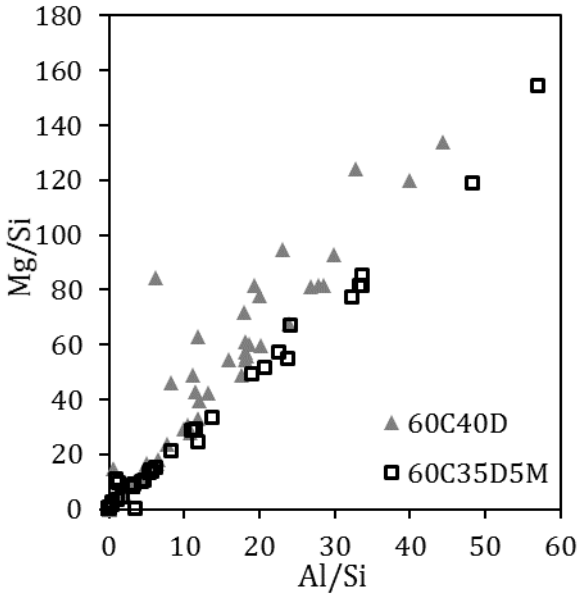

Figure 8: Mg/Si ratio over the Al/Si ratio for the point analyses of the reaction rims around the dolomite grains of samples cured at 60 °C for 360 days.

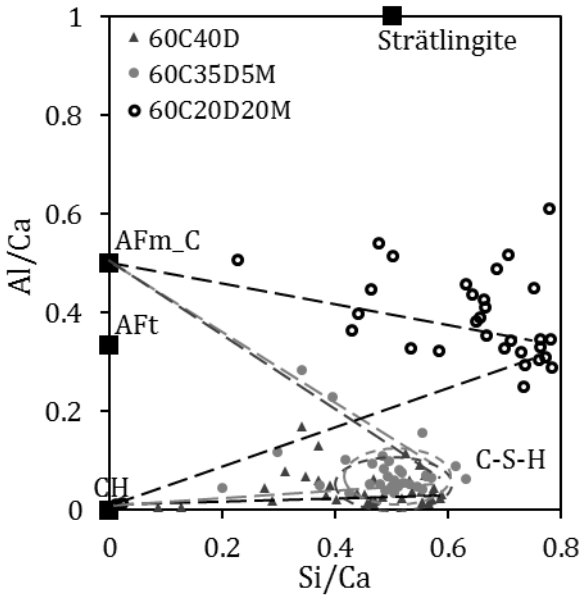

Figure 9: Al/Ca ratio over the Si/Ca ratio for the point analyses of the matrix of samples cured at 60 °C for 360 days.

813

814

815

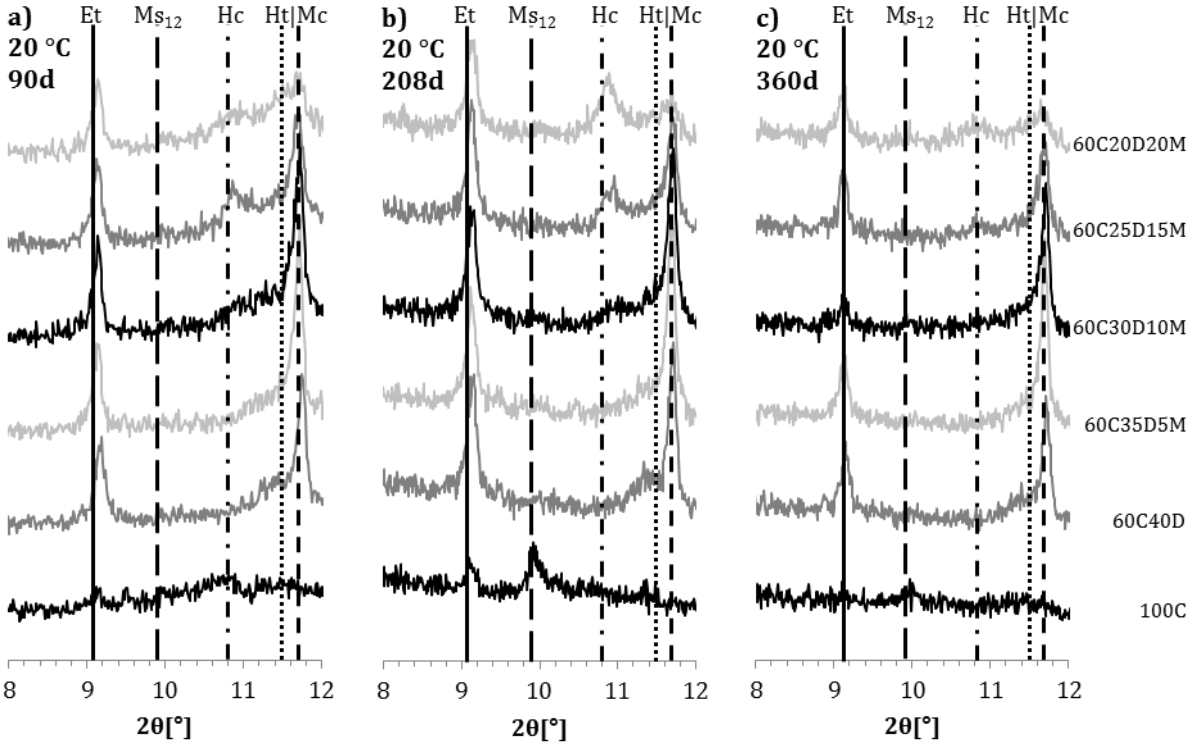

Figure 10: XRD-patterns of samples containing dolomite and the reference (100C) cured at 20 °C for a) 90 days, b) 208 days and c) 360 days.

816

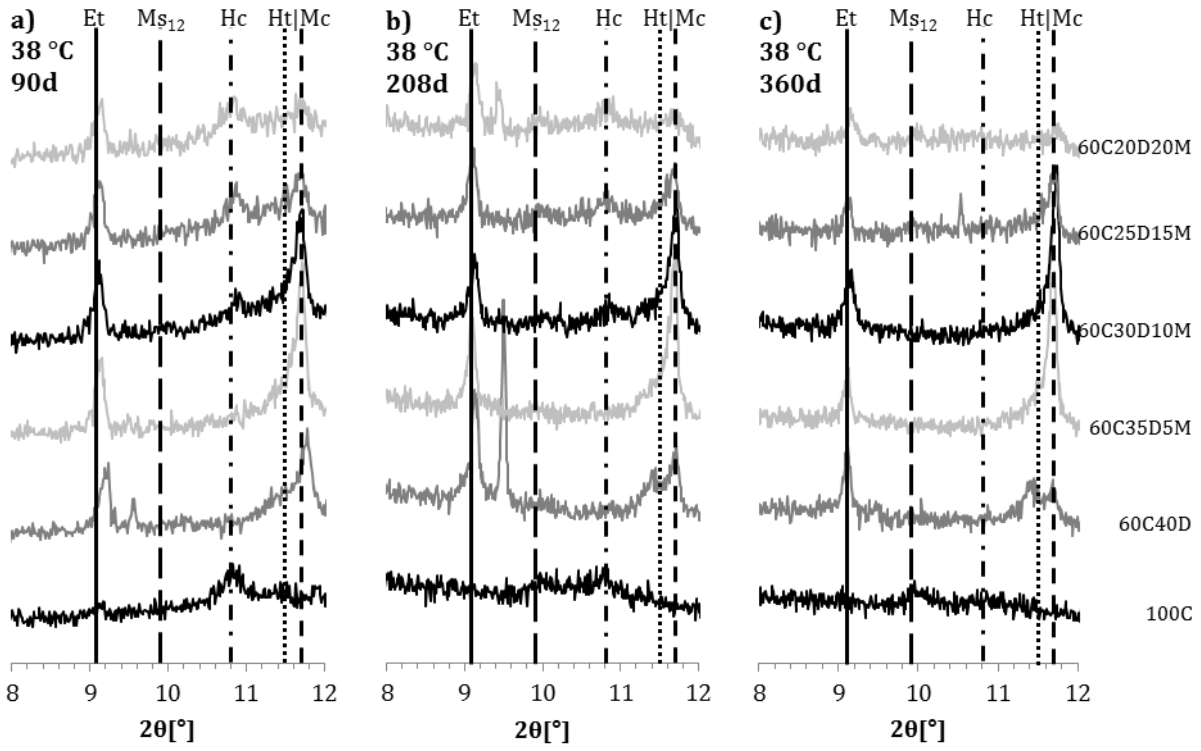

Figure 11: XRD-patterns of samples containing dolomite and the reference (100C) cured at 38 °C for a) 90 days, b) 208 days and c) 360 days.

817

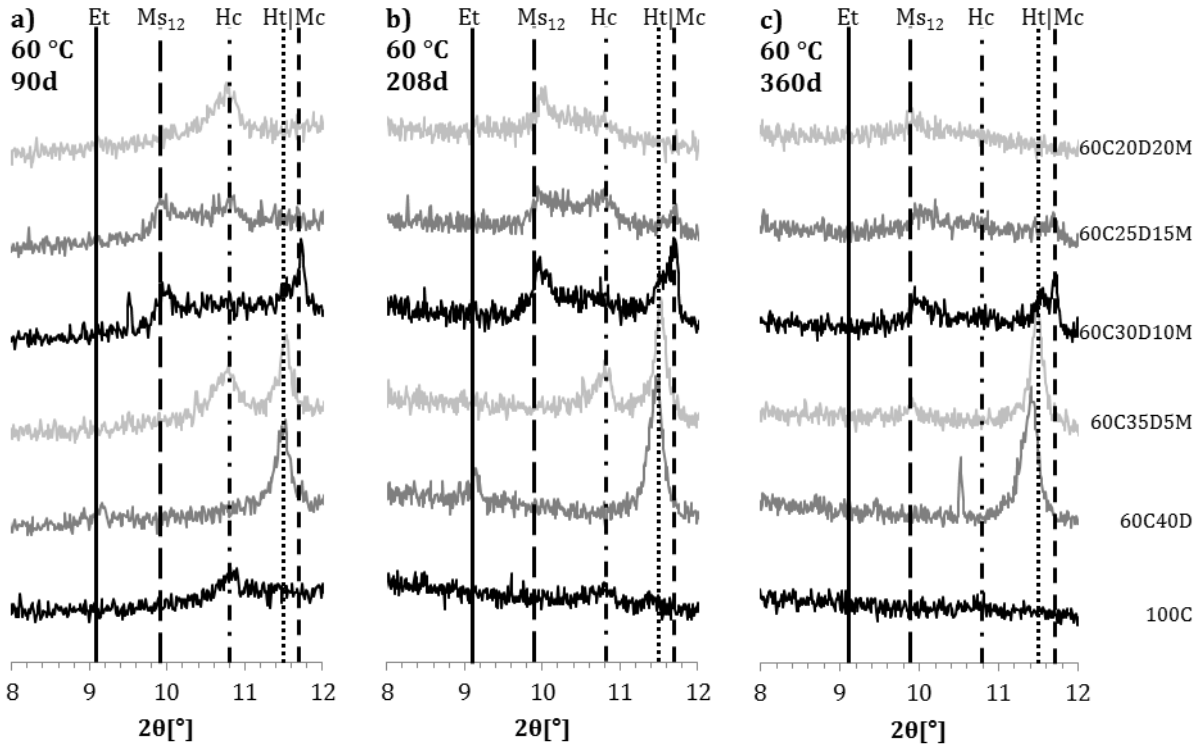

Figure 12: XRD-patterns of samples containing dolomite and the reference (100C) cured at 60 °C for a) 90 days, b) 208 days and c) 360 days.

818

819

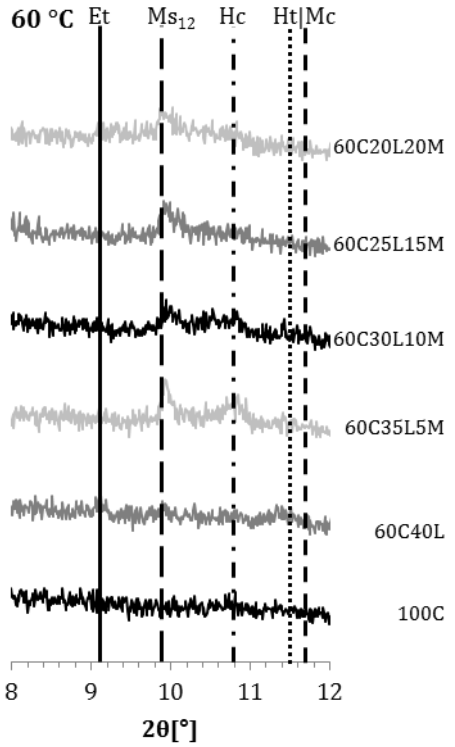

Figure 13: XRD-patterns of samples containing limestone and the reference (100C) cured at 60 °C for 360 days.

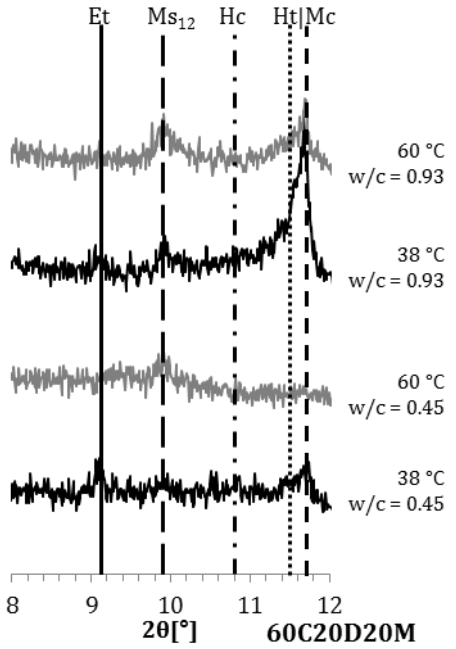

Figure 14: XRD-patterns of the 60C20D20M samples with a w/b ratio of 0.45 and 0.93, cured at 38 °C and 60 °C for 400 d.

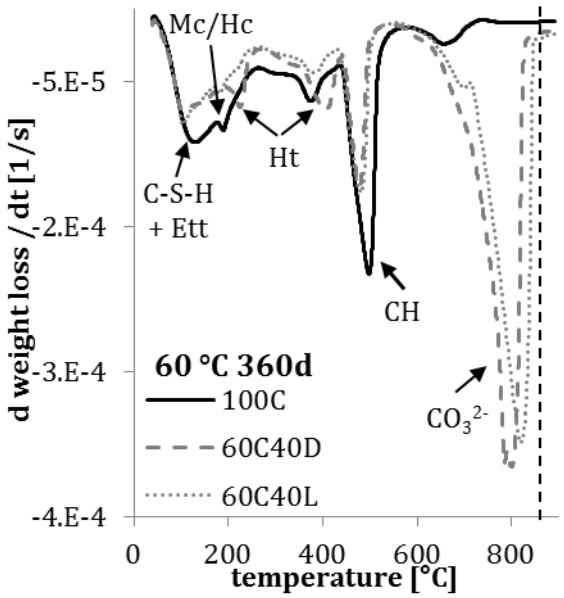

Figure 15: Differential thermogravimetric (DTG) curves for samples 60C40D, 60C40L and the reference 100C cured at 60 °C for 360 days.

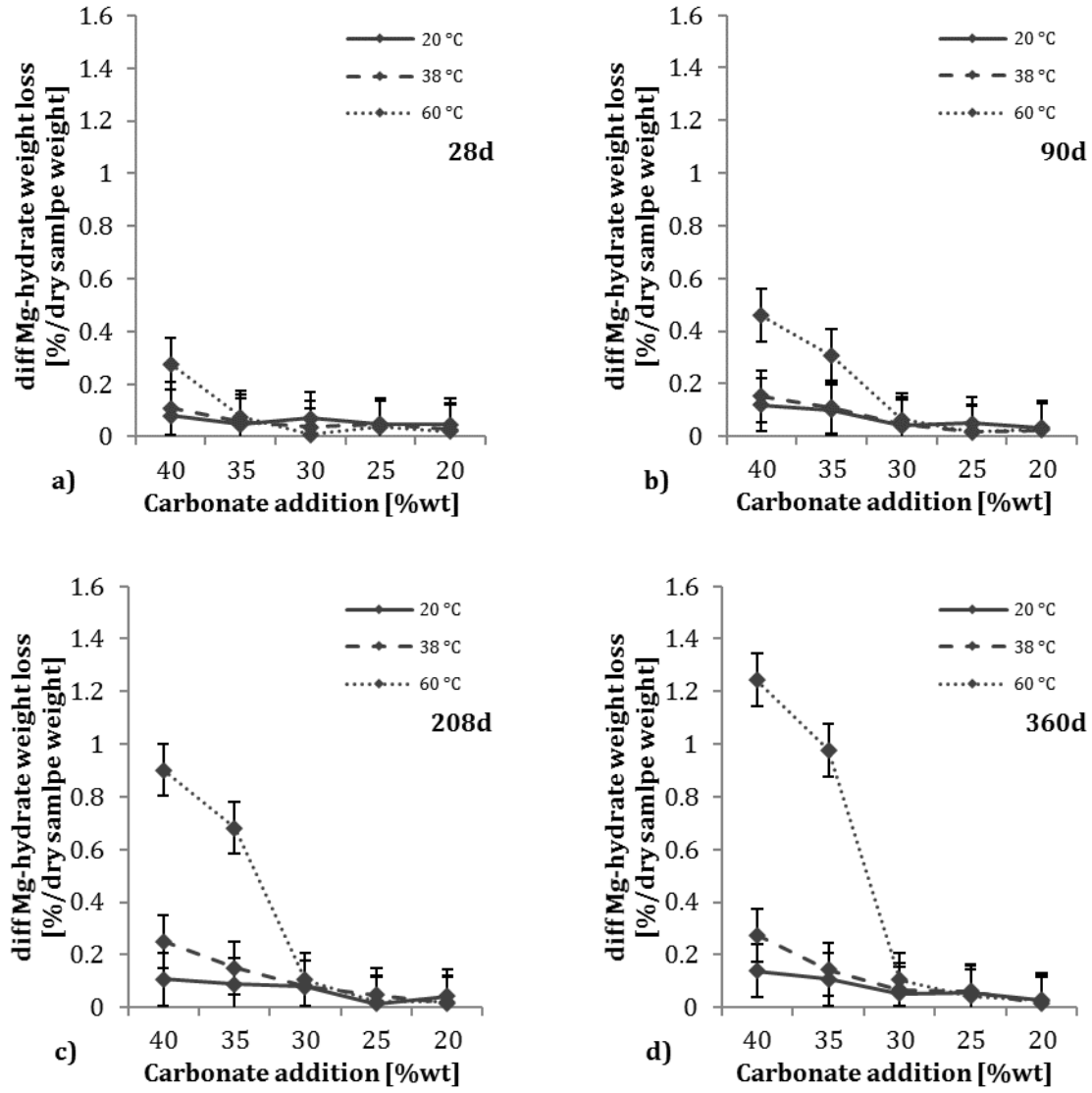

Figure 16: Development of the difference in Mg-hydrate weight losses between samples containing dolomite and samples containing limestone for the various carbonate additions, cured at 20 °C, 38 °C, and 60 °C for a) 28d, b) 90d, c) 208d, and d) 360d. It is important to note that, due the broad shape of the peaks and the possible overlapping of weight loss peaks, these weight losses give only an indication about magnesium-containing hydrates decomposing in this temperature region, not necessarily only hydrotalcite.

824

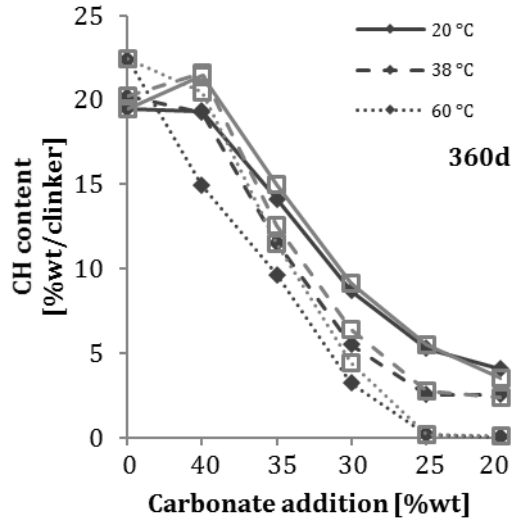

Figure 17: Development of the portlandite content for the samples containing various amounts of dolomite or limestone in combination with metakaolin and the reference 100C cured at 20 °C, 38 °C and 60 °C for 360 days. *Black diamonds* indicate the samples containing dolomite and *grey squares* indicate the samples containing limestone.

825

826

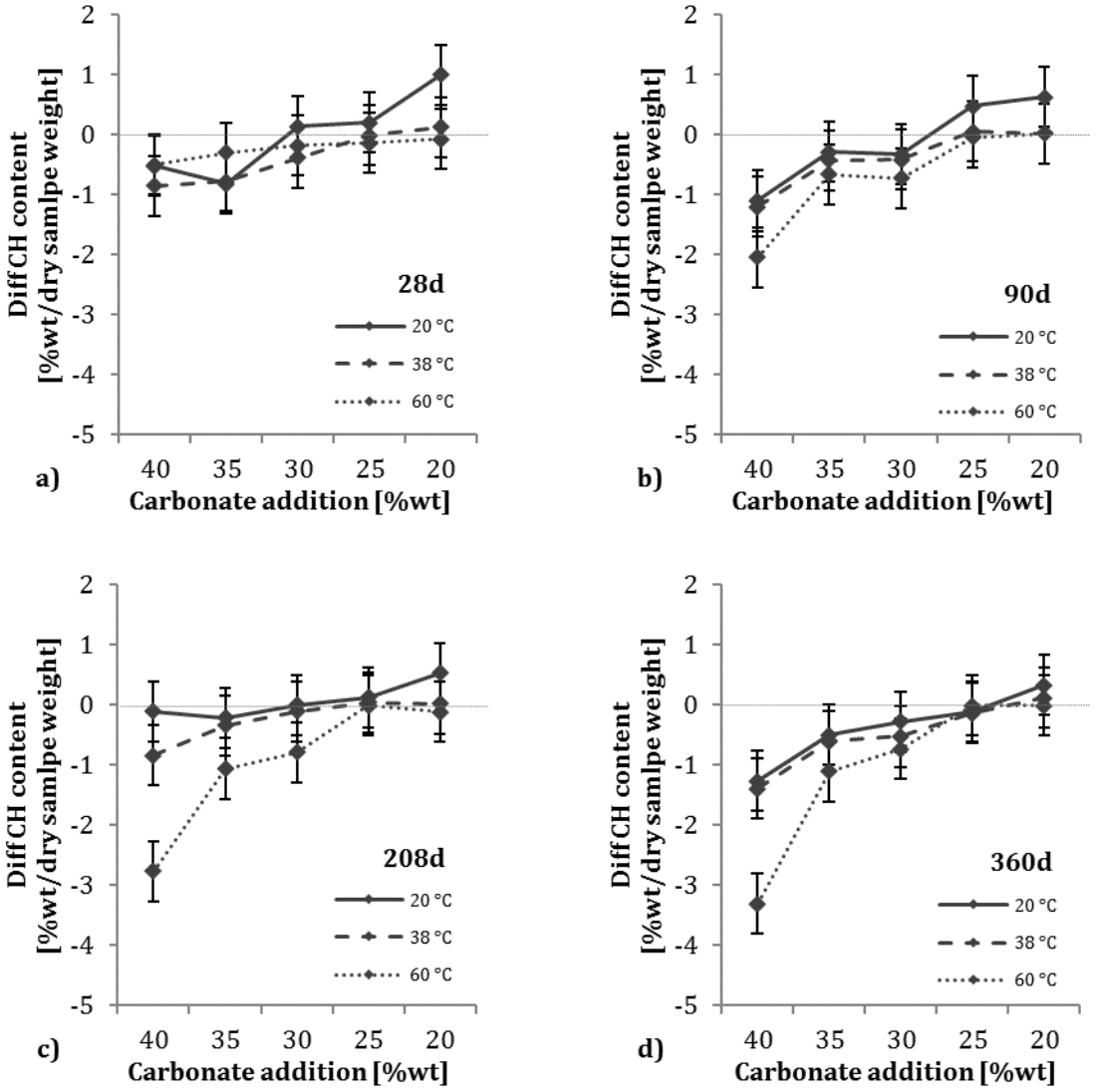

Figure 18: Development of the difference in the portlandite content between samples containing dolomite and limestone for the various carbonate additions, cured at 20 °C, 38 °C, and 60 °C for a) 28d, b) 90d, c) 208d, and d) 360d.

827

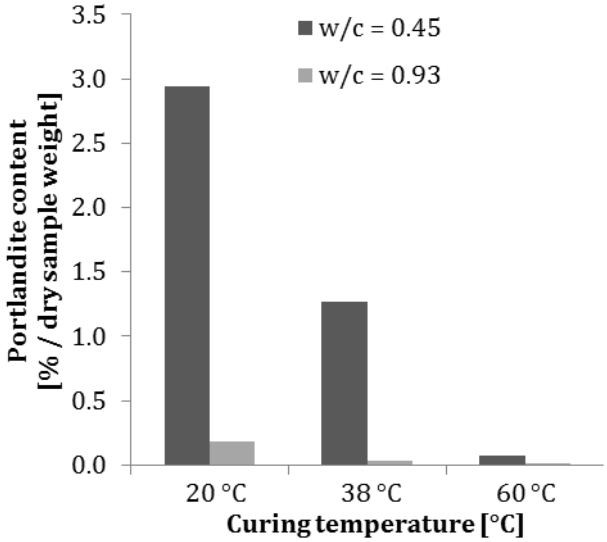

Figure 19: Portlandite content of samples with a w/b ratio of 0.45 and 0.93 cured at 20 °C, 38 °C and 60 °C for 400 days.

828

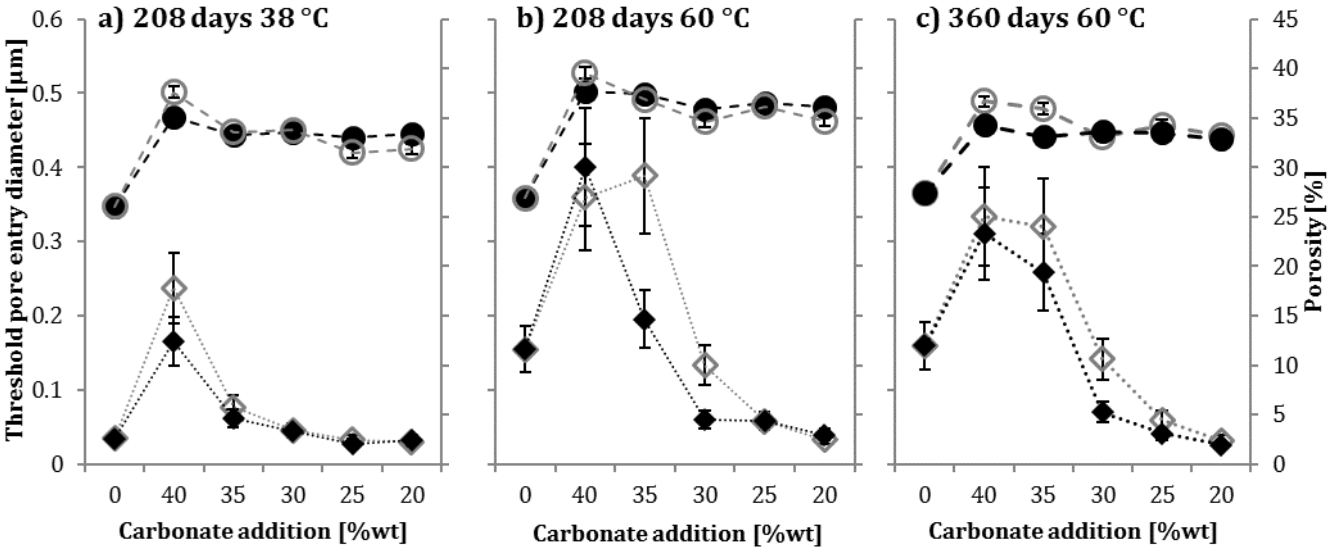

Figure 20: Development of the threshold pore entry diameter (*diamonds*) and porosity (*dots*) for samples containing dolomite (*black filled*) or limestone (*grey hollow*) cured for a) 208 days at 38 °C, b) 208 days at 60 °C and c) 360 days at 60 °C.

829

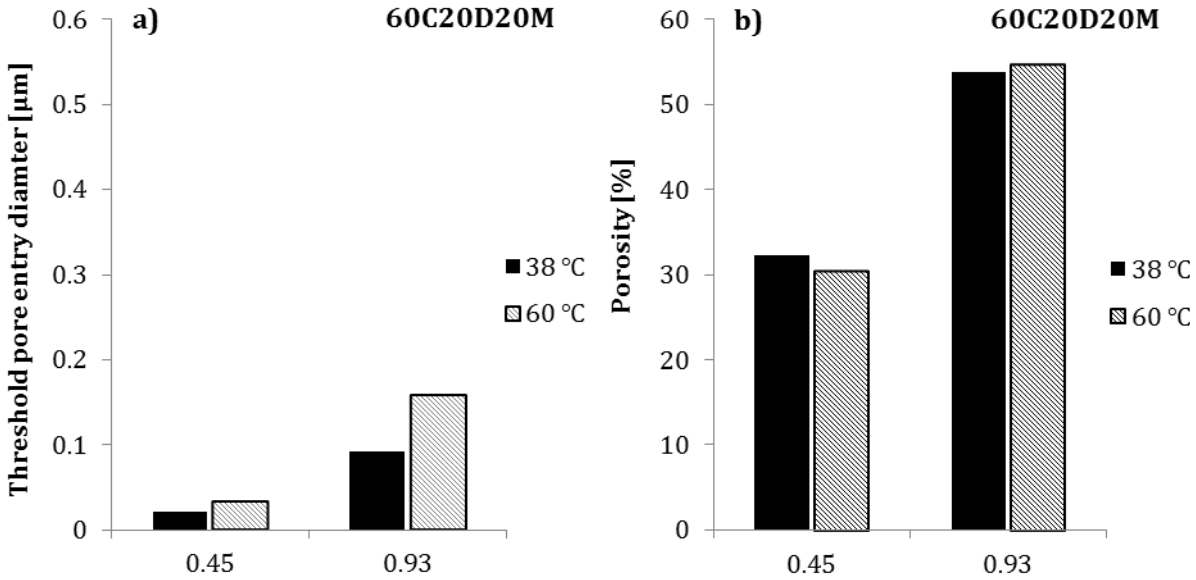

Figure 21: The threshold pore entry diameter (a) and the porosity (b) for the sample 60C20D20M prepared with a high (0.93) or low (0.45) w/b ratio cured at 38 °C or 60 °C for 400d.

830

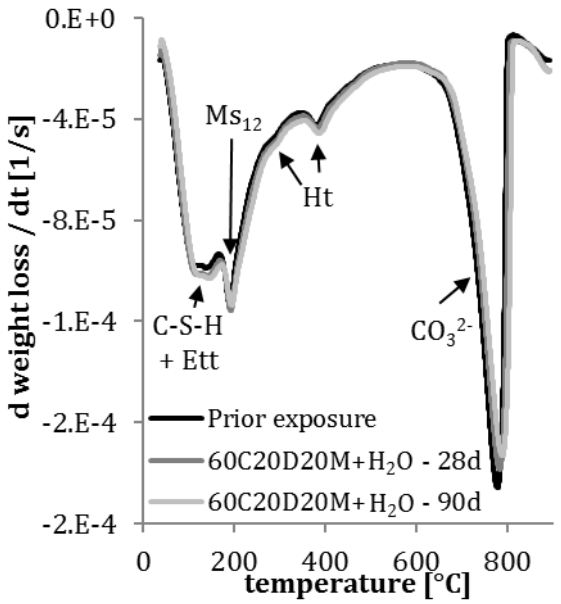

Figure 22: Differential thermogravimetric (DTG) curves for well-hydrated samples 60C20D20M exposed to 30%wt additional water for 28 or 90 days at 60 °C and the sample prior exposure.

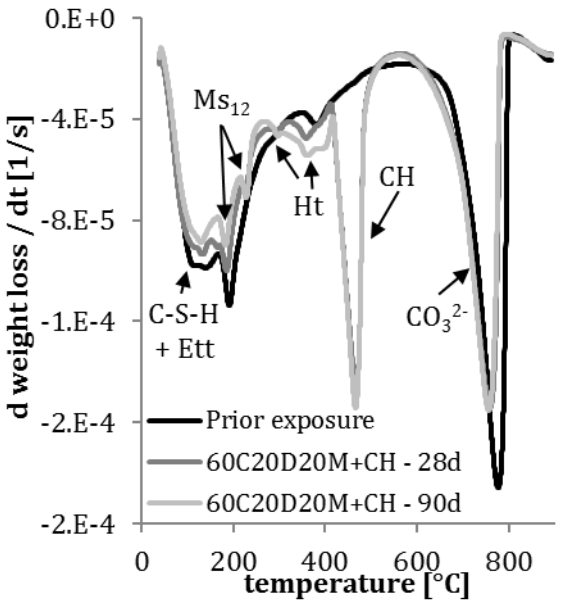

Figure 23: Differential thermogravimetric (DTG) curves for well-hydrated samples 60C20D20M exposed to 30%wt additional water and 30%wt portlandite for 28 or 90 days at 60 °C and the sample prior exposure.

831

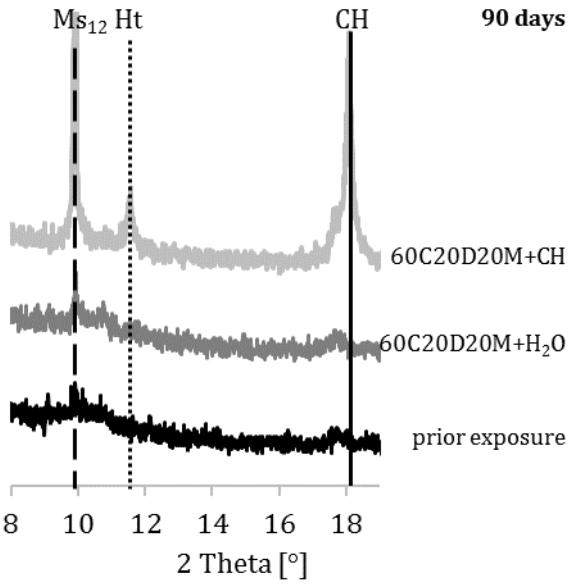

Figure 24: XRD-patterns of the well-hydrated samples 60C20D20M exposed to 30%wt of additional portlandite and or water for 90 days at 60 °C and the sample prior exposure.

832

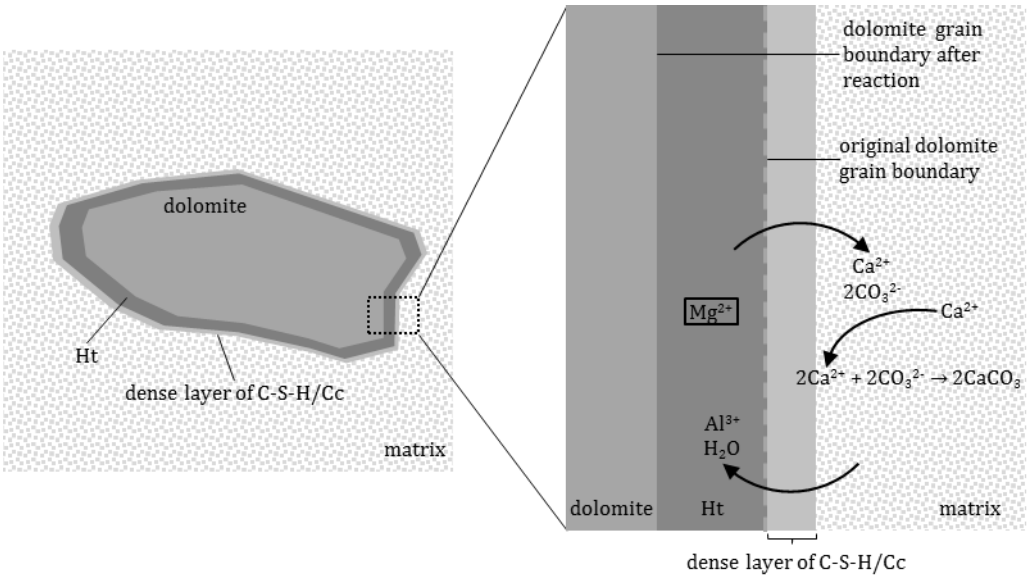

Figure 25: Schematic illustration of the hydrotalcite formation in the reaction rims around the dolomite grains.

833